TRANSIENTS INFLUENCING ROCKET ENGINE IGNITION AND POPPING

INTERIM (14 MONTH) REPORT

UNDER CONTRACT NAS 7-467

APRIL 30, 1969

BY

T.R.MILLS, B.P.BREEN, E.A.TKACHENKO AND B.R.LAWVER

DYNAMIC SCIENCE A DIVISION

OF MARSHALL INDUSTRIES

MONROVIA, CALIFORNIA

PREPARED FOR

NATIONAL AERONAUTICS AND SPACE ADMINISTRATION

TRANSIENTS INFLUENCING ROCKET ENGINE IGNITION AND POPPING

By

T.R. Mills, B.P.Breen,
B.R.Lawver, and E.A.Tkachenko

Interim Report
April 30, 1969
SN-95E

Prepared under Contract NAS7-467
DYNAMIC SCIENCE, a Division
of Marshall Industries
Monrovia, California

for

NATIONAL AERONAUTICS AND SPACE ADMINISTRATION

FOREWORD

This interim report was prepared for NASA Jet Propulsion Laboratory. Project Monitor on this contract was Richard M. Clayton, Liquid Propulsion Section of Jet Propulsion Laboratory, California Institute of Technology, Pasadena, California

This effort was conducted for the Contract NAS7-467 for the period May 1, 1967 to June 30, 1968. Dynamic Science number assigned to this report was SN-95D.

This is the second interim report (14 months) covering a continuing research program being conducted to develop a meaningful model which describes the interrelation of the various physio-chemical processes in establishing the combustion chamber environment during the starting transient and during steady operation.

SUMMARY

The purpose of this work was to determine and demonstrate the effect which rocket engine design and operating parameters have upon high amplitude pressure waves (spikes) associated with vacuum starts using hypergolic propellants. Necessary calculations can be made by a computer program which was synthesized for the solution of the sequence of processes from initial propellant injection to propellant ignition. These processes consist of the injected propellant flow transient, propellant vaporization, and preignition chemistry and lead to early combustor environments which either give smooth ignition or can be conducive to detonative processes. The potential magnitude of the pressure waves can be computed at selected times throughout the chamber pressurization transient.

A preliminary parametric study of vacuum starts determined the effect of initial conditions on chamber pressure, gas temperature, product species, and potential detonation pressure. The effects of various time steps, droplet size distribution, heat transfer between the chamber gases and chamber wall, transient propellant flow, and preignition chemistry on the pressurization history were shown and their physical importance evaluated. Detonation pressure levels were plotted as a function of the time between propellant injection and detonation and as a function of the initial conditions.

In attempting to add coherence to the understanding of random pressure waves encountered in hypergolic propellant systems, a separate study of high pressure waves produced during steady-state combustion (pops) was conducted. The currently available literature and experimental data were used to perform order of magnitude calculations. A possible source of engine roughness or popping was shown photographically to involve injection mixing explosions.

CONTENTS

NOMENCLATURE

A	Arrhenius reaction rate constant, cc/mole-sec for a bimolecular reaction
A_c	Thrust chamber surface area, ft^2
A_o	Flow area through orifices, in^2
A_p	Effective flow area through line, in^2
A^*	Nozzle throat area, ft^2
A_v	Effective flow area through valve, in^2
$\bar{A}_v$	Average valve flow area, in^2
a	Acoustic velocity, ft/sec
C_D	Discharge coefficient
C_{fu}	Concentration of fuel, mole/cc
C_H	Propellant header capacitance
C_L	Propellant line capacitance
C_o	Discharge coefficient through orifices
C_{ox}	Concentration of oxidizer, mole/cc
C_p	Heat capacity at constant pressure, Btu/lb-^oR, cal/gr-^oC
C_{p_l}	Specific heat of reactants before detonation, Btu/lb^oR
$C(t)$	Condensed phase material produced during vaporization in chamber, lb/sec
C_v	Discharge coefficient through valve
D	Diameter of jet, ft
d	Diameter of line, in
E	Activation energy, Btu/lb-mole, cal/gr-mole
E_p	Modulus of elasticity of line lb/in^2
f	Ratio of liquid propellant species to total propellant (liquid and gaseous) species
G_j	Mass evaporated from a single drop in the system during one time interval, lb_m
G_w	Mass of vapor condensed on chamber walls during one time interval, lb_m
g_c	Gravitational constant, 32.2 lb_m-ft/lb_f-sec^2
H	Enthalpy of propellants and products, Btu/lb_m
H_{vap}	Enthalpy of vaporization, Btu/lb
h	Heat transfer coefficients, Btu/sec-ft^2-^oR

$I_{c,e}$	Intermediate condensed phase products produced by preignition chemistry which leave the nozzle
I(t)	Intermediate products produced by preignition chemistry which ultimately lead to ignition
I_v	Intermediate vapor products produced by vapor phase preignition chemistry
$I_{v,e}$	Intermediate vapor phase products produced by preignition chemistry which leave the nozzle
K	Thermal conductivity, Btu/sec-ft^2-(^{o}R/ft)
k	Specific heat ratio
k_1	Specific heat ratio before detonation
k_2	Specific heat ratio after detonation
L	Length of line between valve and propellant tank, ft
L(t)	Two phase flow from orifices, lb/sec
ℓ	Wall thickness of line, in
M	Molecular weight, lb_m/lb-mole
M_1	Mach number before detonation
m_c	Mass of vapor in the thrust chamber, lb_m
m_f	Partial order of reaction with respect to fuel
m_{noz}	Vapor mass efflux through the nozzle, lb_m
N	Number of wave reflections in the propellant line during the valve opening time
N_D	Total number of drops in the system
n	Wave propagation index
n_{FP}	Time interval in which the temperature of a drop reaches the freezing point
n_o	Partial order of reaction with respect to oxidizer
n_x	Time interval in which a drop becomes frozen
P	Pressure, lb/in^2
P_c	Chamber pressure, lb/in^2
$P_c(t)$	Chamber pressure (time variable), lb/in^2
P_D	Chapman-Jouquet detonation pressure, lb/in^2
P_d	Pressure downstream of valve (or vapor pressure if cavitation is present), lb/in^2
P_g	Gas pressure, Psf, mmHg
$P_g(T_g)$	Partial pressure of gas at temperature T_g, Psf
P_m	Manifold pressure, lb/in^2

P_n	Pressure upstream of valve at n^{th} valve area change, lb/in^2
P_p	Plateau pressure (following a Chapman-Jouquet detonation) lb/in^2
Pr	Prandtl number
$P_s(t)$	Spike pressure, lb/in^2
$P_T(t)$	Tank pressure (time variable) lb/in^2
P_{TK}	Tank pressure, lb/in^2
P_v	Propellant vapor pressure, lb/in^2
$P_v(T_{dj})$	Propellant vapor pressure corresponding to the drop temperature, T_d, for the jth drop, Psf.
$P_v(T_w)$	Propellant vapor pressure evaluated at the wall temperature, T_w, Psf
P_1	Pressure before detonation, lb/in^2-a
P_2	Pressure after detonation lb/in^2-a
$\bar{Q}$	Heat release due to chemical reaction minus phase change, Btu/lb
Q_n	Total energy transferred to all drops in the system in one time interval, Btu
$(q_v)_j$	Rate of energy transfer to an ensemble of drops, Btu/sec
R	Universal gas constant, 1546, lb_f-ft/lb-mole^oR, 1987 cal/gr-mole^oK
Re	Reynolds number
$R_o(t)$	Two phase orifice resistance, lb/in^2
R_s	Orifice resistance for vapor sonic flow, lb/in^2
R_v	Valve resistance, lb/in^2
r	Reactor radius, in
r_j	Radius of drops for the j^{th} ensemble, ft
r_{ox}	Amount of oxidizer that reacts, lb_m
$\dot{r}_1$	The reaction rate of a mixture before become compressed
$\dot{r}_2$	The reaction rate of a mixture after being compressed
T	Temperature, ^oR, ^oK
$T_c(t)$	Preignition gaseous chamber temperature, ^oR
T_1	Temperature before detonation, ^oR
t	Time, sec
t_{vo}	Valve opening time, sec
V	Velocity, ft/sec
V_c	Chamber volume, ft^3

V_n	Velocity of propellant through line at n^{th} valve area change, ft/sec
$V_n(t)$	Vapor products produced by liquid vaporization which leaves the nozzle
V_s	Effective velocity of the pressure wave in an elastic line, ft/sec
$V(t)$	Vapors which enter into the preignition chemical reactions
$V_1(t)$	Vapor flow from orifices during sonic flow, lb/sec
$V_2(t)$	Vapor produced in chamber from vaporizing liquid in L(t), lb/sec
$V_e(t)$	Vapor products produced by preignition chemistry
$\mathscr{V}$	Volume, ft^3
v	Specific volume, ft^3/lb
W	Propellant flowed in time Δt, lb
$\dot{W}$	Weight flow of propellant, lb/sec
$\mathscr{W}$	Weight of propellant, lb
X	Mass Fraction, $\dot{W}_g/\dot{W}_t$
X_j	Fraction of drop that is frozen
$\mathscr{X}$	Distance from injector face, in
Y	Liquid mass fraction, $\mathscr{W}_\ell/(\mathscr{W}_\ell+\mathscr{W}_g)$
Z z	Heat transfer factors, dimensionless
Z_L	Line impedance, lb/in^2
α	Accommodation coefficient
β	Volume expansivity of fluid, $^oR^{-1}$
ΔA_v	Valve opening area change in time Δt, in^2
ΔH	Heat of reaction, Btu/lb
ΔP	Pressure drop through flow area, lb/in^2
ΔPi_n	Initial rarefaction wave pressure change for n^{th} initial wave, lb/in^2
$\Delta Pr_{n,m}$	Reflected wave pressure change originating with n^{th} initial wave for the m^{th} reflection, lb/in^2
$\Delta \dot{r}$	The increase in reaction rate due to an isentropic compression
$\Delta t_n, \Delta t$	Length of time interval, sec
ΔV_n	Fluid velocity change in pipe dur to valve area change for the n^{th} valve area change, ft/sec
μ_g	Absolute gas viscosity, lb/sec-sec
ρ	Density, lb/ft^3

τ_e	Heat of vaporization, Btu/lb
τ_f	Heat of fusion, Btu/lb
τ_s	Heat of sublimation, Btu/lb
Φ	Term defined by equation 34
ϕ_n	Area ratio factor between valve and line for n^{th} valve area change (see Appendix B)
ψ_m	Wave reflection factor at partially open valve for m^{th} wave reflection (see Appendix B)

Subscripts:

f	final
g	vapor
i	initial
d_j	drop ensemble
ℓ	liquid
n	time interval
n-1	time interval previous to time interval n
o	initial
ox	oxidizer
t	total (the sum of liquid and vapor)
w	wall
2p	two phase

INTRODUCTION

A troublesome, and at the same time, highly complex phenomenon which is observed during some engine starting transients is the occurrence of high pressure waves, usually termed pressure "spikes." Hard starting characteristics have been encountered in both large scale (Ref. 1) and small scale (Ref. 2) space engine programs and their fixes usually involve trial and error hardware testing rather than attempting to identify the mechanism which causes the hard starts. Similarly, pressure disturbances, commonly referred to as "pops," are known to occur during steady-state rocket engine operation over a wide range of injection parameters (Ref. 3). Various attempts to explain the source of these pressure disturbances have been made, however, most of these attempts are qualitative. Originally it was commonly assumed that explosions of accumulated propellant masses were the cause of the observed pressure waves. As a result of more recent experimental studies, it has been found that under certain conditions detonable chemical reaction intermediates can accumulate in the combustion chamber (Refs. 4, 5, and 6). This fact provides evidence that detonative compounds and mechanisms, increasing the danger of initiating and propagating these pressure waves, must therefore be understood and described.

The main objective of this investigation has been to develop an analytical model describing rocket engine chamber conditions during the start transient. By necessity, the model is semiempirical in nature, that is, containing several parameters which are best evaluated from experiments, or from empirical correlations. The model calculates by mass balances the condition of the propellant species during the low pressure startup history as first shown by Agosta (Ref. 7) and later incorporated into the models of References 8 and 9. The extension which this work has allowed is the identification of individual physical processes and the assignment of mechanistic coefficients of importance. The model thus depends on previous hypergolic research on ignition mechanisms (Refs. 4 and 10) and on ignition chemistry (Refs. 5, 6, and 11). Thus, the intent and contribution of the present study is to provide an analytical mechanistic framework which will allow theoretical parametric studies to be made. These studies can point out which parameters theoretically affect chamber behavior most significantly and, thus, will give direction to the experimental measurement of these parameters. The phenomena of steady-state popping and

starting spikes may be related to the basic nature of ambient or low temperature hypergolicity, thus, although the analytical modeling of these phenomena are separate tasks, mechanistic understanding of either may give insight to the other.

The transient start model accounts for complete nonuniformity in time history and is uniform within the chamber space; it is based on time dependent differential equations formulating physical and chemical processes governing conditions. The set of equations consist of:

1) transient flow equations,
2) vaporization, freezing, and pressurization equations,
3) chemical kinetic equations which include concentration and temperature dependence, and
4) chemical reaction equations

The actual solution of these equations is carried out numerically by a finite difference method and the computer program is arranged such that each of the cited sets of equations is treated as one unit. Typical start sequences have been analyzed and effects on pressurization, preignition chemistry, ignition delay and detonation potential were determined for certain parametric variations

The modeling of steady-state popping involved order of magnitude calculations which showed that observed waves could only be accounted for by propagation through a detonable mixture. The amplitude of detonation waves originating at different points in the rocket chamber was calculated and a mechanism of possible detonation initiation was identified and is shown photographically to involve injection mixing explosions

TECHNICAL DISCUSSION

During vacuum starting transients and steady-state operation of hypergolic liquid rocket engines, high amplitude overpressures frequently occur. Since both start-transient overpressures (spiking) and steady-state over-pressures (popping) are often observed with hypergolic propellant combinations both overpressure mechanisms may be due to the basic nature of hypergolicity. Two basic points are involved in the nature of hypergolicity: first, low activation energies are involved, (often leading to complex intermediates) and second, the ignition reaction is exponentially dependent on temperature in the region of hypergolicity. Either overpressure condition may result in hardware damage or may initiate combustion instability and thus it is important to understand their causes and similarities. The spiking phenomena apparently can occur with any nitrogen based hypergolic propellant and may be associated with the formation of reaction intermediates under the conditions of low initial chamber pressure and correspondingly low temperatures. The popping phenomena may be initiated by injection transients involving both the mixing processes and sudden liquid phase reaction.

These two phenomena were investigated in a joint effort in order to relate any understanding of hypergolic reaction, gained from one phenomenon, to both problems and where possible to make use of interrleated data in the literature which were recorded in the study of one phenomenon but which gives insight into the other. A two-fold effort was undertaken: (1) a model of the processes involved in the vacuum start transient was formulated so that conditions at any time could be calculated and (2) motion picture data and mechanism calculations pertinent to the popping phenomena were made. The majority of effort was expended in improving and parametrically demonstrating the vacuum start model developed in previous work (Refs. 7, 8, and 9). Significant data were also gathered from the identification of mix/separate phenomena during the recent hypergolic impingement work (Ref. 12) performed at Dynamic Science under contract to NASA/Lewis.

Specifically, the following modifications were to be made to the vacuum start model of Reference 1, so that parametric studies of the processes affecting the spike overpressure level could be made:

1) Variable propellant mass flow rate (time dependence can be of any prescribed functional form, e.g., linear, nonlinear, step function and may include system dependence related to predictable pressure surges caused by the propellant feed system dynamics and chamber pressure feedback; either propellant may have a prescribed injection lead and transient).

2) Preignition chemical reaction of propellants (the stoichiometry, reaction mechanism, and reaction rate were included to permit parametric studies, as well as allow inclusion of new chemical kinetics and mechanism data furnished by experiment).

3) Heat transfer from the combustion chamber gases to the propellant droplets (Priem correlation), and heat transfer between the chamber wall and the combustion chamber gases (by means of effective heat transfer coefficients).

4) Prediction of the vacuum ignition overpressure and detonation level based on what has been calculated to be in the chamber by the flow vaporization, and preignition models. Since the program now prints out the chemical species in the chamber it will be possible to correlate not only the overpressure amplitude but the species detonation sensitivity.

Insight into the popping phenomena was gained when it was noted in the concurrent research of Reference 12 that hypergolic streams mix at low temperature but exhibit roughness with large impingement contact time. High speed motion pictures of this phenomena demonstrated that this roughness was due to injection mixing explosions which randomly broke up the spray pattern and sometimes lead to complete spray detonation.

Mathematical Analysis of Start Transient

The interrelationship of the various physical and chemical processes which determine the transient conditions during vacuum starting are shown in Figures 1 and 2. The three main processes are described individually so that mechanism models of transient flow, vaporization (heat transfer) and preignition chemistry can be developed. While description of this overall interaction involves a computer accounting model developed during previous work (Refs. 8 and 9) the controlling parameters of the individual processes were the subject of the improvement effort reported here.

Transient Propellant Flow, Analytical (I)

The mathematical analysis of the transient flow system is herein described from the propellant tank to the injection of propellants into the combustion chamber.

The tank pressure can assume any function of time, for this analysis it is assumed constant. The opening of the propellant valve sets up a pressure surge in the propellant line between the tank and the valve. This pressure surge consists of a series of pressure and rarefaction waves which move up and down the propellant line and are eventually damped out by friction and reflection losses at either end of the line. There are several methods for solving these hydraulic transient problems (Refs.13 and 14); each method being applicable to a particular type of problem. Steady oscillatory problems can be solved by transient flow equations, but transient-flow problems cannot be solved by steady-oscillatory equations, therefore, the methods available for solution are: (1) arithmetic, (2) graphical, (3) method of characteristics, and (4) algebraic. The method of characteristics and algebraic methods require computers for solution, and are therefore rather complex. The graphical method is developed easily by plotting in a two-dimensional plane. The arithmetic method is simplest, does not need a computer for a solution, will not add a great deal of complexity to the existing vaporization program and, therefore, will be adapted for use in this analysis.

The arithmetic method neglects friction and the procedure solves a simplified, linearized form of the momentum and continuity equations. Figure 3 shows the construction of the time varying pressure upstream of the valve for the cases when $t_{\text{valve open}} \leq 2L/V_s$ (Figure 3b) ("instantaneous valve opening) and $t_{\text{valve open}} > 2L/V_s$ ("slow" valve opening), (Figure 3c). For most cases encountered in attitude control engines, valve opening is nearly instantaneous. The procedure for determining the time varying pressure is as follows:

The valve is assumed to open linearily, i.e., the valve open area varies linearily with time. For valve opening times greater than $2L/V_s$ (the time required for a wave to travel from the valve to the tank and back again), the opening time is divided into time increments of $2L/V_s$. During each time increment, a rarefaction wave is sent up the line. The time varying pressure is the sum of these rarefaction (and reflected compression) waves (Figure 3 c.). The initial rarefaction wave pressure drop is obtained from:

$$\Delta Pi_n = \frac{\rho_\ell V_s}{g} \Delta V_n \ , \tag{1}$$

Figure 3 a. The first initial wave, ΔPi_1 is reflected from the valve end of the line unchanged in magnitude(to maintain continuity and simplicity of construction). In reality, all reflected waves lose some of their strength at the valve end due to the partially opened valve (A fully closed valve would reflect the wave fully and a fully open valve, whose opening presents a smooth bore to the pipe, would transmit the wave through it unchanged in magnitude or direction.).

All subsequent reflected pressure waves are calculated from:

$$\Delta Pr_{n,m} = \Psi_m \Delta Pi_n \ , \tag{2}$$

Figure 3a. Initial rarefaction waves are sent out at intervals of $2L/V_s$ until the valve is full open. For valve opening times less than or equal to $2L/V_s$, a single rarefaction wave is sent out.

Propellant flow through the valve is now controlled by a time varying pressure upstream of the valve and, for noncavitating flow, the pressure downstream of the valve. Although the flow through the valve is highly transient, a steady-state type of flow rate equation will be used to determine the flow through the valve. Since the instantaneous rate controlling pressures will be used in the equation, this approximation should not introduce a gross error. Accordingly, the velocity in the line upstream of the valve is determined by:

$$V_n = C_v \Phi_n \left[\frac{2g}{\rho_\ell} (P_n - P_d) \right]^{1/2} \tag{3}$$

which is related to the change in velocity by:

$$V_n = V_o + \sum_{i=1}^{i=n} \Delta V_i . \tag{4}$$

The orifice flow rate will be controlled by the upstream pressure as long as the fluid is cavitating within the valve, i.e., the static pressure has dropped below the vapor pressure due to low manifold pressure and/or high fluid velocity through the valve. As long as the flow is cavitating, the downstream pressure, P_d, is constant and equal to the vapor pressure P_v.

Initially, the volumes downstream of the valve, the propellant manifold and the combustion chamber will be at zero pressure (hard vacuum of space). As the valve opens and the propellants become exposed to the vacuum, the liquid accelerates toward the injector. As the liquid expands into the vacuum a portion of the liquid flash vaporizes, filling the manifold, and flows out of the orifices. The vaporizing liquid and the cold hardware reduces the bulk temperature of the entering liquid, and in some cases solid propellant may form. The entering propellants will continue to vaporize until the manifold pressure reaches the vapor pressure corresponding to the bulk temperature of the entering propellants or until the manifold is filled with the entering liquid. The vaporized propellant escapes from the liquid surface to pressurize the manifold and also small gas bubbles become entrained within the liquid to form a vapor-liquid suspension. If the manifold pressure is low and the residence time of the suspension is long, the vapor will stay in suspension. As the manifold becomes pressurized, however, the vapor may become dissolved in the liquid or may condense. The vapor-liquid suspension has a low bulk modulus which results in a soft, pressure absorbing element in the system, therefore, as more mass flows into the manifold the suspended vapor bubbles will collapse.

An analysis of the time varying two-phase mixture in the injector manifold is extremely difficult to perform. Complicating the analysis is the dependence of vapor formation on heat transfer from the hardware to the mixture and the spatial orientation of the vapors and liquid within the manifold. It appears, therefore, that the most expeditious approach to this portion of the analysis is to construct a typical manifold and perform a series of tests using suitable instrumentation. The current analysis, therefore assumes that: (1) immediately after the valve opens the downstream pressure influencing flow through the valve is equal to the vapor pressure of the entering propellants and that this pressure remains constant until the manifold is full; (2) the vapor-liquid

mixture enters the manifold at a constant quality until the manifold is full; (3) the vapor-liquid mixture temperature drops to an assumed temperature due to cold hardware and self-cooling from vaporization, and; (4) the manifold filling can be calculated by integrating a steady-state flow rate equation. The flow rate equation is:

$$\dot{W} = C_V A_V \sqrt{2g \rho_\ell \Delta P} \quad . \tag{5}$$

For nonvariable flow conditions, the amount flowed in time Δt is:

$$W = C_V A_V \sqrt{2g \rho_\ell \Delta P} \quad \Delta t \tag{6}$$

If the area of the valve is changing only, the amount flowed is:

$$W = C_V \bar{A}_V \sqrt{2g \rho_\ell \Delta P} \quad \Delta t \quad . \tag{7}$$

If the downstream pressure is constant but the upstream pressure changes linearily, then Equation (5) can be integrated to give the amount flowed as:

$$W = \frac{2}{3} \frac{C_V A_V \sqrt{2g\rho_\ell}}{(P_n - P_{n-1})} \left[(P_n - P_V)^{3/2} - (P_{n-1} - P_V)^{3/2} \right] \Delta t \quad . \tag{8}$$

Finally, if the upstream pressure and valve area simultaneously are changing linearily, then the integration of Equation (5) gives:

$$W = \frac{2}{5} \frac{C_V \Delta A_V \sqrt{2g\rho_\ell}}{P_n - P_{n-1}} \left[(P_n - P_V)^{3/2} - (P_{n-1} - P_V)^{3/2} \right] \Delta t \quad . \tag{9}$$

Following the determination of the pressure upstream of the propellant valve, the manifold filling time is determined from the appropriate equation (one of equations 6 through 9) by substituting the weight of propellant when the manifold is full into one of equations 6 through 9.

The transient manifold pressure is determined from the continuity equation by equating flow into and out of the manifold. If it is assumed that the fluid properties are constant and the flow rate is expressed by a flow type equation, a reasonably simple expression can be written for the pressure inside the manifold:

$$P = \frac{1}{(C_v^2 A_v^2 + C_o^2 A_o^2)} \left[C_v^2 A_v^2 P_n + C_o^2 A_o^2 P_c \right]. \tag{10}$$

Where eqn. (10) is substituted into the steady orifice flow, the following results:

$$\dot{W}_{orifice} = (2g\rho_\ell)^{1/2} \left[\frac{C_o^2 A_o^2}{(C_v^2 A_v^2 + C_o^2 A_o^2)} (C_v^2 A_v^2 P_n + C_o^2 A_o^2 P_c) - P_c \right]^{1/2}. \tag{11}$$

The injector propellant flowrate can now be expressed in terms of the transient pressure surge upstream of the propellant valve after the manifold is full of propellants and the chamber pressure determined from the vaporization program.

Transient Propellant Flow, Experimental. - (I)

The experimental effort was directed at investigating the effects of propellant cavitation on propellant flow rate. It was felt that transient cavitation at the valve and later at the injector orifices controlled the propellant flow into the injector during the start transient.

In order to experimentally define the cavitating injector orifice discharge coefficient, a controlled set of tests was conducted. A single stainless steel orifice with $d_i = .030$ inch, and $L/D = 10$ was tested with N_2O_4. The propellant temperatures ranged between 32^oF and 110^oF, and chamber pressures ranged between .25 psia and atmospheric pressure. A discharge coefficient was defined by:

$$C_D = \frac{\dot{W}_{measured}}{\dot{W}_{theoretical}} \tag{12}$$

where

$$\dot{W}_{theoretical} = A_o \sqrt{2g\ \rho_\ell \Delta P} \tag{13}$$

and ΔP used in equation (13) is: $\Delta P = P_{manifold} - P_v$ when $P_c \leq P_v$, and $\Delta P = P_{manifold} - P_c$, when $P_c > P_v$. Discharge coefficients described by equation (12) varied between .56 and .86. General agreement with the trends predicted by theoretical analysis of noncavitating orifices was observed.

In order to check the experimental results, theoretical estimates of the discharge coefficient were made. As long as an orifice was cavitating the two phase mixture was flowing at the two phase sonic velocity. Two phase flow rate and acoustic velocity through an 0.30 inch orifice were plotted versus mass fraction, S, ($\dot{W}_{gas}/\dot{W}_{total}$) for N_2O_4 and N_2H_4 for various temperatures, (Figures 4 and 5). The derived equations for theoretical flow rate and acoustic velocity are:

$$\dot{W}_{2p} = \frac{\rho_\ell A_o}{\left[\frac{1}{a_\ell^2} + \left(\frac{\rho_\ell}{\rho_g}\right)^2 \frac{1}{a_g^2} X\right]^{1/2}} \tag{14}$$

and

$$a_{2p} = \frac{1+\frac{\rho_\ell}{\rho_g} X}{\left[\frac{1}{a_\ell^2} + \left(\frac{\rho_\ell}{\rho_g}\right)^2 \frac{1}{a_g^2} X\right]^{1/2}} \tag{15}$$

if it is assumed that $X << 1$. For temperatures, pressures, and flow rates characteristic of normal operation of a typical space start engine, the mass fraction, from Figure 4, lies in the range from 10^{-4} to 10^{-6}. It is seen, therefore, that the two phase acoustic velocity (Figure 5) is near a minimum, and at high mass fractions, 10^{-4}, yields reasonable values of velocity through an orifice. At low mass fractions the velocity through the orifice approaches the liquid acoustic velocity, that is, from equation (15),

$$\lim_{X \to 0} a_{2p} = \frac{1}{[1/a_\ell^2]^{1/2}} = a_\ell . \tag{16}$$

This velocity is not a realistic limit since the liquid acoustic velocity approaches 6000 ft/sec. To correct this discrepancy the following substitution was made in eqn. (14) and used in correlating the experimental data to calculate the theoretical flow rate.

$$a_\ell = V_\ell = C_o \sqrt{2g \frac{\Delta P}{\rho_\ell}} \tag{17}$$

To determine the mass fraction of gas generated during cavitation an isentropic process was assumed so that:

$$X = - \frac{(T_f)_\ell C_{p\ell} \mathrm{Ln} \frac{(T_f)_\ell}{(T_i)_\ell} - v_\ell \beta_\ell (T_f)_\ell (P_f - P_i)}{H_{vap_\ell}} \tag{18}$$

As long as X is small (of the order of 10^{-4} or less) $(T_f)_\ell$ will be nearly equal to $(T_i)_\ell$, so for cavitating flow:

$$X = \frac{v_\ell \beta_\ell (T_i)_\ell (P_f - P_i)}{H_{vap_\ell}} \tag{18a}$$

Combining equations (14), (17), and (18a), eliminating a_ℓ and X to define a two phase flow rate and employing equation (13) to define a theoretical flow rate, a theoretical discharge coefficient can be defined as:

$$C_D = \frac{\dot{W}_{actual}}{\dot{W}_{theoretical}} = \frac{\dot{W}_{2p}}{\dot{W}_{theoretical}} \tag{19}$$

By choosing an orifice discharge coefficient, C_o, of 1.0 and 0.7, a plot of C_D vs P_c was constructed for various propellant temperatures (Figure 6). From Figure 6 it is seen that the experimental discharge coefficients fall within the range of the theoretical discharge coefficients and therefore nominal theoretical coefficients may be used for cavitating and noncavitating flow alike. The results of these analyses have not yet been incorporated into the Transient Pressure History Program. Programming of those equations necessary to describe the transient propellant flow will be undertaken in the coming year's follow on to this work.

Vaporization Program. - (II)

The pressurization of a thrust chamber is treated mathematically as a sequence of steady-state processes in very short time intervals. At the start of each new time interval, a new set of drops enter the thrust chamber. These drops undergo vaporization during the time interval as do the drops which entered previously. At any time, each drop has a unique radius, temperature and physical state (solid fraction). The equations used in this part of the program (vaporization) were outlined by Agosta (Ref. 7) and later incorporated into computer programs by Seamans, et al (Ref. 8) and Dynamic Science (Ref. 9).

Based on the kinetic theory of gases, the mass evaporated from a single drop in one time interval is given by:

$$G_j = [P_v(T_{dj})_{n-1} - P_g(T_g)_{n-1}] \quad \alpha (r_j)^2_{n-1} \Delta t_n \sqrt{\frac{8\pi M g_c}{R(T_{dj})_{n-1}}} \tag{20}$$

where $P_v(T_{dj})_{n-1}$ is the vapor pressure corresponding to the temperature of the j^{th} drop at the end of the previous time interval. Therefore, the total mass evaporated in one time interval is obtained by summing all G_j for that particular interval.

Condensation on the chamber wall can occur if the gas pressure exceeds the propellant vapor pressure evaluated for the wall temperature. The mass of vapors condensing on the chamber walls in one time interval is given by:

$$G_w = [P_g(T_g)_{n-1} - P_v(T_w)] \alpha A_c \Delta t_n \sqrt{\frac{M g_c}{2\pi R(T_g)_{n-1}}} \tag{21}$$

with the constraint $0 \leq G_w < \infty$.

The vapor mass flow through the nozzle during one time interval for a constant k is given by:

$$m_{noz} = (P_g)_{n-1} A^* \Delta t_n \sqrt{\frac{k M g_c}{R(T_g)_{n-1}} \left(\frac{2}{k+1}\right)^{\frac{k+1}{k-1}}} \tag{22}$$

The mass of vapor in the chamber at the end of the n^{th} time interval is obtained from the perfect gas law.

$$(m_c)_n = \frac{V_c M}{R} \left[\frac{P_g}{T_g}\right]_n \tag{23}$$

The temperature of the gas in the chamber at the end of the n^{th} time interval is evaluated by obtaining a mass weighted average. For a single species system with constant vapor heat capacity, the temperature is given by:

$$(T_g)_n = \frac{\sum_{j=1}^{n} G_j (T_{dj})_{n-1} + (T_g)_{n-1}\left[(m_c)_{n-1} - (G_w)_n - (m_{noz})_n\right] - \frac{Q_n}{C_{pg}}}{\sum_{j=1}^{n} G_j + (m_c)_{n-1} - (G_w)_n - (m_{noz})_n} \tag{24}$$

where Q_n is the total heat transferred from the vapor to all drops in the system during one time interval.

The gas partial pressure in the chamber at the end of the n^{th} time interval is therefore:

$$(P_g)_n = (T_g)_n \left[\frac{P_g}{T_g}\right]_{n-1} + \frac{R}{V_c M}\left[\sum_{j=1}^{n} G_j)_n - (G_w)_n - (m_{noz})_n\right] \quad (25)$$

where $(T_g)_n$ is evaluated from equation (24).

New drop radii and drop temperatures must be calculated at the end of each time interval to account for the effect of evaporization on the size and temperature of each drop. The radius at the end of each time interval is given by:

$$r_j = (r_j)_{n-1}\left[1 - \frac{3.\left[P_v(T_{dj})_{n-1} - P_g(T_g)_{n-1}\right]\alpha\Delta t_n \sqrt{\frac{M g_c}{2\pi R(T_{dj})_{n-1}}}}{\rho_\ell (r_j)_{n-1}}\right]^{1/3} \quad (26)$$

The new drop temperature is obtained from an energy balance on the drop, including the effect of heat transfer from the vapors to each drop. The heat transfer rate to the drop is:

$$(q_v)_j = 4\pi h (r_j)^2_{n-1} Z \left[(T_g)_{n-1} - (T_{dj})_{n-1}\right] \quad (27)$$

where

$$Z = \frac{z}{e^z - 1} \quad (28)$$

$$z = \frac{G_j C_{pg}}{4\pi h \Delta t_n (r_j)^2_{n-1}} \quad (29)$$

$$h = \frac{K_g}{2(r_j)_{n-1}}\left[2 + .6\ Pr^{1/3}\ Re^{1/2}\right] \quad (30)$$

$$Pr = \left[\frac{C_p \mu}{K}\right]_g \quad (31)$$

and

$$Re = \frac{2(r_j)_{n-1} V_{drop} M (P_g)_{n-1}}{\mu_g R (T_g)_{n-1}} \quad (32)$$

where the temperature of each drop is:

$$(T_{dj})_n = (T_{dj})_{n-1} - \sqrt{\frac{M g_c}{2\pi R(T_{dj})_{n-1}}}\left[\frac{3\left[P_v(T_{dj})_{n-1} - P_g(T_g)_{n-1}\right]\alpha (r_j)^2_{n-1} \tau_e \Delta t_n}{C_{p\ell}(r_j)^3_n \rho_\ell} + \Phi\right]. \quad (33)$$

where

$$\Phi = \frac{3h[(T_g)_{n-1} - (T_{dj})_{n-1}] \; Z \; (r_j)^2_{n-1} \; \Delta t_n}{\rho_\ell C_{p\ell} (r_j)^3_n} \quad . \tag{34}$$

The solid fraction of the drop, X_j, increases in successive intervals until the drop completely solidified. The equation of X_j is given by:

$$X_j = \sum_{n=n_{FP}}^{n_x} \left[\frac{3 \; G_j \tau_s}{4\pi\rho_\ell (r_j)^3_n \tau} - \frac{C_{p\ell}}{\tau} \Phi \right] \tag{35}$$

The total energy reaching the surface of all drops in the system in one time interval, Q_n, is given by:

$$Q_n = \sum_{j=1}^{n} (q_v)_j \Delta t_n \; N_D \tag{36}$$

where N_D is the total number of drops in the system.

Thus far the discussion has been concerned with only one species, i.e., either fuel or oxidizer injection. However, the program has the ability to calculate both fuel and oxidizer injection with either propellant injected at a given point in time.

When fuel and oxidizer are both being injected, reactions take place and products are formed. From kinetic theory the amount of oxidizer which reacts, r_o in a given time step, n, is given by:

$$(r_{ox})_n = \sqrt{6} A M \left[\frac{(C_{ox})_{n-1}}{V_c} \right]^{n_o} \left[\frac{(C_{fu})_{n-1}}{V_c} \right]^{m_f} e^{-\frac{E}{R(T_{average})}} \tag{37}$$

where

$$(C_{ox})_{n-1} = \frac{((P_g)_o)_{n-1} \; V_c}{R(T_{average})} \quad , \text{ and} \tag{38a}$$

$$(C_{fu})_{n-1} = \frac{((P_g)_f)_{n-1} \; V_c}{R(T_{average})} \quad . \tag{38b}$$

Several analytical studies were conducted to improve the operation of the vaporization program and to make it more realistic. These studies investigated the effect of (1) the time step size (2) the number of initial drop sizes, and (3) the heat transfer between the combustion chamber gases and the chamber wall. Mechanistic additions to the program to make it more realistic were (1) preignition reactions, and (2) variable propellant flow rate (by means of tabulated flow rates versus time and/or an orifice flow equation which depends on the chamber pressure).

Variable Time Step: Figures 7 and 8 show the effects of time step size on chamber pressure and gas temperature for a stepwise flowrate of N_2O_4 only into the chamber. During each excursion the time step was held constant at the values indicated.

The early influence of the integration step size on chamber pressurization is shown in Figure 7. A significant difference in pressurization history is obtained as a result of employing a time increment of 25×10^{-6} sec. as compared to time increments ranging from 0.5×10^{-6} to 4×10^{-6} sec. Reduction of the step size from 1.0×10^{-6} sec to 0.5×10^{-6} sec produces no significant change in pressurization behavior during the early pressurization period (0 to 0.2 msec).

Figure 8 shows the very strong effect of integration time step size on the chamber gas temperature. The time increments must be reduced to values less than 2×10^{-6} sec before relatively small temperature differences are obtained as a result of decreasing the time step.

From these results it appears that a relatively small time step is needed, at least initially, so that the time step does not adversely influence the model of the physical process. These results also indicate that a time step as small as 1×10^{-6} sec is needed; however, a step this small results in high computing costs for reasonably long runs. As a result, a variable time step scheme illustrated in Figure 9 was used. This scheme is a compromise between initially small time steps for modeling accuracy and eventually large time steps for low computer costs.

Drop Size Distribution: The vaporization model was initially set up with a drop size distribution containing three radii of 7.00×10^{-4}, 2.05×10^{-3}, and 4.61×10^{-3} inches, each radius representing respectively 30%, 40%, and and 30% of the total propellant injected. This scheme also resulted in high computing costs. In an effort to reduce these costs a comparison between the three drop distribution and a one drop distribution of radius 2.05×10^{-3} inches was made (Fig. 10). Nitrogen tetroxide only was injected and from these results there appears to be very little difference in chamber pressure between these two distributions. As a result, the vaporization program now uses a single droplet model having a radius of 2.05×10^{-3} inches.

Heat Transfer: As a further refinement to the vaporization program, heat transfer between the combustion chamber gases and the combustion chamber wall was considered. Heat balances are performed on the vaporized propellants before they react and subsequently a heat balance is performed on the combustion product gases. The heat balances now appear as: $_{p}Q_{\text{vaporized}} + {}_{p}Q_{\text{chamber gases}} + {}_{p}Q_{\text{wall to gases}} = {}_{p}Q_{\text{condensed}} + {}_{p}Q_{\text{nozzle}}$ for the propellant vapors, and $_{R}Q_{\text{newly reacted}} + {}_{R}Q_{\text{chamber gases}} + {}_{R}Q_{\text{wall to gases}} = {}_{R}Q_{\text{condensed}} + {}_{R}Q_{\text{nozzle}}$ for the reactant product vapors. The term which has been added is $Q_{\text{wall to gases}}$ which may be positive or negative, depending on the relative temperatures of the gases and the combustion chamber wall.

Preignition Chemistry. -

Preignition chemical reactions were considered so that ignition could ultimately be achieved. The analytical framework for treating preignition chemistry is as follows: the vapor reaction stoichiometry, heat of reaction and rate of reaction are governed by chamber temperature and reactant vapor partial pressures which are continually computed and followed by the vaporization program. Within this framework, the chemical findings of Stevens (Ref. 10) and Weiss (Ref. 11) are incorporated in the sometimes parallel or series paths along with the controlling physical mechanism limits measured by Zung (Ref. 4). In order to analytically describe the experimentally determined change of the kind and relative quantity of reaction products with vapor temperature and vapor O/F, ten temperature regimes, each of which consists of two concentration regimes, have been incorporated into the computer program.

The numerical data for the low temperature regimes ($T < 530^{\circ}$ R) have been furnished by the results of work under contract NAS7-438, Mod. 3 (Ref. 4) which involved the chemical quantitative analysis of the N_2O_4/N_2H_4 preignition reaction products. A schematic representation of how the computer program is able to treat preignition reaction paths is as shown on the following page. On the basis of chemical quantitative analysis carried out under contract NAS7-438, Mod. 3, and data from Reference 15, three temperature regimes were actually employed to check out the computer program. Although the stoichiometry and therefore $\Delta H_{\text{reaction}}$ for certain temperature and concentration regimes for

$400 \leq T \leq 530^{\circ}R$

$O/F \leq .5 \qquad \Delta H = 1123$ Btu/lb

$$9N_2O_4 + 25N_2H_4 \rightarrow 10N_2O + NO + 19NH_3 + 3\tfrac{1}{2}N_2 + 4H_2O + 7N_2H_5NO_3$$

$O/F > .5 \qquad \Delta H = 2220$ Btu/lb

$$63N_2O_4 + 64N_2H_4 \rightarrow 80N_2O + 16NO + 11N_2 + 72H_2O + 28NH_4NO_3$$

$530 < T \leq 600^{\circ}R$

$O/F \leq .5$ and $O/F > .5 \qquad \Delta H = 2605$ Btu/lb

$$2N_2O_4 + 4N_2H_4 \rightarrow 2N_2O + NO + 2\tfrac{1}{2}N_2 + 2H_2O + NH_4NO_3 + 4H_2$$

$600 < T \leq 10{,}000^{\circ}R$

$O/F \leq .5$ and $O/F > .5 \qquad \Delta H = 4860$ Btu/lb

$$N_2O_4 + 2N_2H_4 \rightarrow 3N_2 + 4H_2O$$

$E = 7500$ cal/gmole

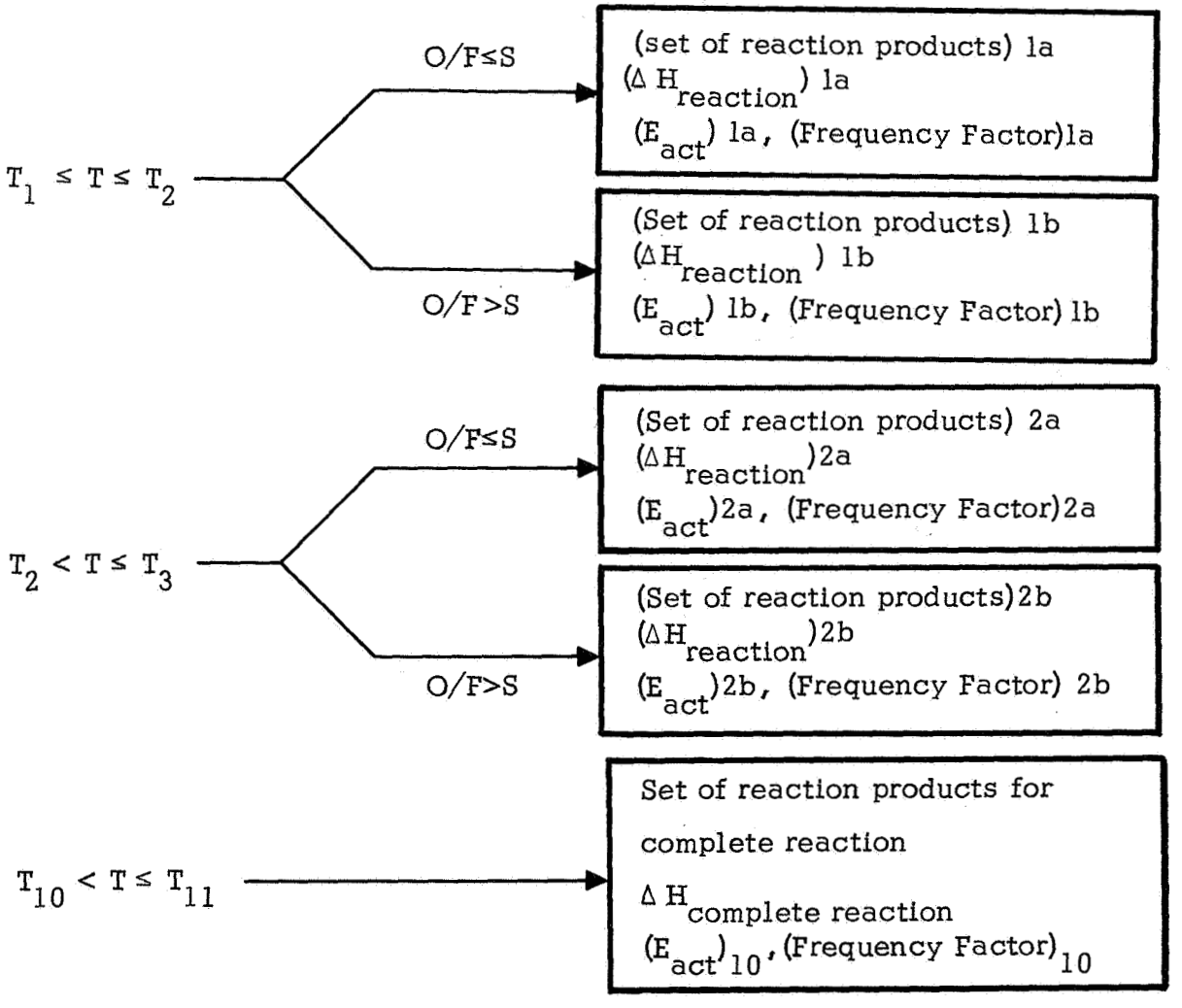

where, T = gas temperature,

S = stoichiometric oxidizer to fuel ratio

N_2O_4/N_2H_4 are presently known, the reaction rates must be estimated, or their effect studied parametrically. Another possibility consists of considering chemical reaction of the vapors to be instantaneous, so that heat release and pressurization by gaseous reaction products is governed by stoichiometry and the kinetics of the system then involve time accounting in stepping through the stoichiometric heat balances. The reaction paths currently programmed and the values of the reaction constants are shown schematically on page 17.

Detonation Program. -

Following the running of the vaporization program to ignition or for a specified time, detonation properties were computed for various selected times. Detonation properties were calculated by the NASA/Lewis detonation program given in Reference 16. This program is well documented in References 16 and 17, so a discussion of the basic principles used is not needed here. To fit the data from the vaporization program to the detonation program some modifications to the data are necessary. The detonation program is written for gaseous reactants while the reactants calculated by the vaporization program contain liquid droplets in a gaseous atmosphere. Table II is a tabulation of some of the data calculated from the vaporization program; the f listed in Table II is the ratio of a liquid propellant species to the total propellant species (liquid and gaseous). This f factor is used to convert the liquid propellant to a pseudo equivalent amount of gaseous reactants. Inherent with this conversion is that all of the liquid will be consumed in the detonation process.

All of each propellant species is converted to vapor reactants having a molecular weight in the ratio: weight of liquid + weight of vapor propellant/ weight of vapor propellant, $(W_\ell + W_g / W_g)$. The new propellant enthalpy is obtained by adding the gaseous molar enthalpy to the liquid molar enthalpy which has been corrected by the liquid to vapor ratio: $[H = H_\ell + H_g (W_\ell / W_g)]$. Thus each liquid propellant species is converted to a pseudo vapor wherein the molecular weight and enthalpy are obtained as outlined above.

Start Transient Results

Appendix A is a listing of the Transient Hypergolic Ignition Program as it currently exists and is described in this report. By using the output (chemical species, species mass fraction, temperature, and pressure) from this program as input to the NASA/Lewis detonation program at specified times, a profile of potential spike conditions can be determined. In order to establish the current capability of the program and present spiking (detonation) data which may be checked with experimental results, a series of trial runs were made. Variable initial starting conditions were programmed (Table I) for the Transient Program with the resulting output at 1, 2, and 3 ms (or ignition) used as input to the detonation program. Table II shows the data used as input to the Transient and Detonation Programs and the output from the Detonation Program. Figures 11 through 14 show chamber pressure and temperature versus time for the initial conditions given in Table I.

With the current mechanistic stoichiometry and for conditions wherein there was no propellant lead, ignition occurred within 4.0 ms if either the oxidizer, fuel, or wall temperature was 580°R(120°F), Figures 11, 12, and 13. When fuel or oxidizer leads were employed ignition occurred within reasonable time delay only when fuel was lead and all temperatures (fuel, oxidizer, and chamber wall) were at least 540° R, (Figure 14).

Figures 15 through 18 show the detonation pressure levels achieved after running the NASA/Lewis detonation program, the input being modified to account for the presence of liquid propellant droplets. Table II also lists the detonation pressure level (Chapman-Jouquet, P_D) and the ideal-gas, constant volume, plateau pressure level, P_p, following the detonation wave. The detonation pressure, while being almost twice the plateau level, is of very short duration. The detonation pressure is not steady but trails off exponentially, in most cases stopping all further propellant flow into the chamber. The plateau pressure, however, lasts longer and is therefore capable of more damage to the chamber (greater work potential). The ratio of the detonation pressure to the plateau pressure (P_D/P_p) is nearly constant ($P_D/P_p \approx 1.87$) for all of conditions in Table II, therefore the detonation pressure level was used in Figures 14 through 18 to illustrate the trends obtained. Figures 15 and 16 show the effect of

propellant leads on detonation pressure. The time scale indicates time from the introduction of the second propellant, i.e., for a 2 ms lead, 1 ms on the time scale indicates 3 ms real time, or 1 ms after the introduction of the lagging propellant (for no lead, the time scale indicates real time).

For the same delay time following the lagging propellant an oxidizer lead results in higher detonation pressures than does a fuel lead and a fuel lead produces higher detonation pressures than does a no lead condition. Furthermore, for all lead conditions, the longer the delay in time to the detonation the higher the detonation pressures that are produced. If it is assumed that the probability of detonation is approximately equal at the same delay time, detonation pressures will result in descending order with oxidizer leads, fuel leads, and finally no leads.

Figures 17 and 18 show the effect of propellant temperature on detonation pressure. Figure 17 is a plot of detonation pressure versus fuel temperature. Indicated on the plot are the corresponding oxidizer temperature and the sampling time used. As the delay time to detonation is increased (1ms to 2ms, and 2 ms to 3 ms) it is apparent that the detonation pressure increased with propellant accumulation. The detonation pressure decreased with increasing full temperature (500° to 580°R) but if detonation pressure is plotted versus oxidizer temperature (Figure 18) no trend is apparent. Detonation pressure was also plotted versus wall temperature and it was found that detonation pressure was not a function of wall temperature for the range of temperatures studied (500° to 580°R).

Popping

Random high amplitude pressure disturbances, commonly referred to as "pops" have been observed to occur during steady-state rocket engine operation with hypergolic propellants. "Popping" is undesirable because it is a possible trigger source for initiation of high frequency combustion instability. The purpose of this phase of the work was to analyze existing "popping" data and to postulate controlling mechanisms.

Engine Test Data. -

The "popping" data currently available is that of Clayton (Ref. 3) Marshall Burrows (Ref. 18) and more recently the work performed under contract NAS7-467, Task 4 (Ref. 12) at Dynamic Science. Clayton's work was performed using an 18 inch diameter engine with variable propellant injection near the chamber wall.

The "popping" was observed by Clayton during the course of a combustion instability test program using N_2O_4/A-50. The hardware used on this program consisted of a multiple doublet element injector with a set of outer doublets manifolded separately to provide independent flow control near the chamber wall. The outer ring of doublets was designed for an O/F of 1.27 to provide a cooler boundary layer gas. The main doublets were designed for an O/F of 2.11. Clayton observed the "popping" in the 18 inch diameter engine after baffles had been added to the injector to eliminate combustion instability. Prior to the addition of the baffles the engine was inherently unstable. The baffles prevented steady-state instabilities from developing, however, the random "pops" were observed.

The occurrence of the "pops" was found to be related to the oxidizer concentration in the outer set of injector doublets which provides the boundary flow. The "pops" could be eliminated by decreasing the oxidizer flow in the outer doublets. It was found also that elimination of the boundary flow resulted in the elimination of the "pops."

The "pops" were found to exhibit the characteristics of a detonation wave, the same as the steady-state instability wave previously reported by Clayton and Rogero (Ref. 19). The "pops" are steep fronted waves with rise times of a few μseconds and pressure ratios across the wave as high as 7:1.

A modification to the boundary flow injector hydraulics was made to insure hydraulically stable propellant streams but, although the severity of the randomly rough combustion was reduced, spontaneous resonant combustion still occurred occasionally when no baffles were employed. Evidence of stream separation was also found by changing the manifolding of the propellants in the boundary flow.

The results of this work show that:

1) "Pops" exhibit the chacteristics of a detonation wave.
2) Conditions in the boundary region exhibit a controlling influence on engine "popping" and resonant combustion.
3) Injector hydraulics influence the "pops."

Two-Phase Detonations. -

If the "pops" are detonation waves, then they must have an initiation source and a mechanism for supplying energy at a sufficiently high rate to drive the wave. In a liquid propellant rocket engine, the energy source exists as unburned vaporizing propellants near the injector face. It has been shown by Nichols, et al (Refs. 20-21) that detonation waves can be supported by burning liquid fuel sprays. They also show the effect of fuel drop size on the detonation velocity (Ref. 21). Droplets as large as 940μ give velocities very close to the Chapman-Jouquet detonation velocities. This is much larger than the average droplet size found in rocket engines, therefore, it is reasonable to expect that detonation velocities within rocket engines would be close to the Chapman-Jouquet velocity.

The detonation pressure ratio was calculated as a function of distance from the injector face, using Dynamic Science's steady-state combustion program in conjunction with Ragland, Dabora, and Nicholl's detonation model (Ref. 20). The calculations were made for the N_2O_4/MMH system at an O/F = 2. The fraction of propellant vaporized as a function of distance from the injector face is tabulated below:

Distance from Face, χ Inches	Per cent Unburnt Material
0.25	93.0
0.50	88.0
0.75	82.0
1.00	78.0
3.00	57.5
5.00	47.0
7.00	40.0
9.00	36.0

The two-phase detonation wave equations:

$$M_1^2 = 2\left(\frac{k_2^2 - 1}{k_1 - 1}\right) \frac{\bar{Q}}{C_{p1} T_1} \tag{39}$$

and

$$\frac{P_2}{P_1} = \frac{1+\gamma k_1 M_1^2}{1 + k_2} \tag{40}$$

where

$$\gamma = \frac{1}{1-Y} \quad Y = \text{mass fraction of liquid.} \tag{41}$$

where used to calculate the detonation pressure ratio. $\bar{Q}$ was modified by multiplying the heat of reaction by the per cent of unburned materials. The value for k_1 was taken as 1.4. The specific heat ratio, k_2, and the steady-state temperature, T_1, were taken from the NASA-Lewis detonation computer program. The value of γ was determined from the vaporization data tabulated above. Figure 19 shows the large effect which unburnt material and droplet number concentration can have on detonation overpressures near the injector face.

It is evident that conditions for heterogeneous detonations are present within the rocket engine and only require an initiation source.

Detonation Sensitivity and Temperature Zones. -

It is recognized that the processes occurring during a heterogeneous detonation involve both physical and chemical processes. However, it seems reasonable to believe that the probability of onset of a detonation is determined

by the chemical reaction rate of the vapor phase mixture because it is this phase which is most readily combusted.

Considerable work has been aimed at defining the onset of a detonation in premixed gases (i.e. Ref. 22 and 23). The Results of this work show that limits on the onset of detonation are imposed by reaction rate limitations and there is some time, called inductance distance, required for the establishment of a stable detonation wave.

It has been found that the induction distance depends on ignition source, mixture composition, pressure and temperature, and the container geometry at the point of ignition. Recently Busch (Ref. 24), has performed an analysis of the initiation process for a heterogeneous detonation of hydrazine and gaseous oxygen. His analysis was performed by letting a simple isentropic compression wave pass from the burned gas into the unburned mixture. The results show the dependence of pressure history on the mixture composition, temperature, and pressure.

If the reaction rate of an unburned mixture determines the probability of the onset of detonation then the probability of detonations can be described by a sensitivity factor.

The ability of a reacting media to respond to a pressure pulse is determined by the reaction rate sensitivity, which is defined as the increase in reaction rate due to an isentropic compression divided by the undisturbed reaction rate, i.e.: Sensitivity = $\Delta \dot{r}/\dot{r}$.

We can determine this sensitivity from order of magnitude calculations as plotted in Figure 20. The sensitivity factor may be expressed as:

$$\frac{\Delta \dot{r}}{\dot{r}} = \frac{\dot{r}_2}{\dot{r}_1} - 1 \tag{42}$$

where

$\dot{r}_2/\dot{r}_1$ = the ratio of the reaction rate of the compressed mixture to the undisturbed mixture the expression for this ratio is:

$$\frac{\dot{r}_2}{\dot{r}_1} = (P_2/P_1)^{1/k} \, e^{E/RT\left[1-(P_2/P_1)^{1-k/k}\right]} \tag{43a}$$

for a first order reaction and

$$\frac{\dot{r}_2}{\dot{r}_1} = (P_2/P_1)^{2/k} \, e^{E/RT\left[1-(P_2/P_1)^{1-k/k}\right]} \tag{43b}$$

for a second order reaction.

A plot of the reaction rate sensitivity was made for a second order reaction with an activation energy of 40 Kcal/mole, (Fig. 20). A wave having a pressure ratio of 1.2 was chosen.

The sensitivity is seen to increase rapidly with decreasing temperature. This indicates that a requirement for high sensitivity is a low reactant temperature, which one might expect near the injector face and also along the chamber wall, particularly in the case of fuel cooled walls. In any engine, the gases adjacent to the wall near the injector face will, in general, be cooler than the bulk as shown in Figure 21. The dependence of sensitivity on temperature may in part explain the role of the chamber wall and material in this region on the "popping" phenomenon. It appears that low amplitude pressure disturbances might be sufficient to initiate a detonation wave in the regions of high sensitivity.

Shock Wave Decay. -

It has been postulated that the "pops" may be due to the explosion of pockets of unburned propellants. This possibility was investigated with a simplified analysis of the expansion of a volume of explosives. A given volume of explosive was assumed to bum to completion within the volume and then expand either isentropically or isothermally. It was found that in either case the pressure decays extremely rapidly and approaches the ambient pressure within a short distance. The results of these calculations were presented in Reference 9.

These results indicate that if the "pops" are the result of a blast wave from an explosion of a pocket of unburned propellant, then, the explosion must either occur very near the pressure transducer or the pocket must be very large, otherwise, it would not be observed with high amplitude. It is, therefore, unlikely that the "pop" is a blast wave, but rather a detonation wave which was initiated by a relatively low amplitude local disturbance.

Hypergolic Stream Mixing and Explosions. -

At Dynamic Science injection mixing explosions were observed during the atmospheric testing of an N_2O_4/N_2H_4 single doublet injector (Ref. 12). The objective of this work was to experimentally determine the limit of hypergolic stream separation for impinging liquid N_2O_4/N_2H_4 streams using both two-dimensional and circular jets. The two-dimensional apparatus allowed photographic observation of both the impingement point and the propellant spray from which separation was determined. An analytical model was developed and correlated the streams mixing or separating regions. However, at conditions of low temperature and long interfacial residence time, it was observed that the mixed ligaments tended to explode before full atomization. The regions of separation/mixing and injector mixing explosions are shown in Figure 22.

Injection mixing explosions (IMES) were found to occur when the circular jets are operated in the mix regime at D/V values greater than about $.9x10^{-4}$ sec. The IMES were characterized by loud repetitive noise similar to machine gun fire. This phenomena was believed to be the same as that observed by Marshall Burrows (Ref. 18),using a small rocket engine. High speed photographs taken by Marshall Burrows clearly show repetitive explosions occurring near the impingement point, however, the photographs were not sufficiently detailed to allow investigation of the phenomena.

Based on the Dynamic Science work it was postulated that a chamber "pop" is a result of a two-phase detonation caused by ignition and explosion within the mixed liquid ligaments. These occur at lower velocities and propagate into the impingement point. The ignition results in an explosion because the propellants are well mixed. It is therefore postulated that two conditions for injector popping must be met:

1) Propellant temperatures must be in the mix regime;
2) Jet breakup time must be long enough to allow ignition within the liquid ligaments.

Experimental Mixing Explosions. -

A set of injector tests were run to verify the postulations of injection mixing explosions and subsequent two-phase detonations. The tests were run using 0.050 inch diameter jets at atmospheric pressure and high speed color photography to observe the impingement region. The photography was accomplished with high intensity front and back lighting using standard photoflood lights. The camera was run at 2000 pictures/second with a 1/20 shutter which gave an exposure time of 25μsec.

The propellants were conditioned to operate in the mix regime. Examination of the film shows intermittent violent explosions within the impingement region. It was found that injection mixing explosions varied in severity, but essentially two types were identified. These are shown in Fig. 23. The first type occurred more frequently and was milder, it is characterized by shattering of the liquid ligaments. The second and more severe explosions appeared to result in complete detonation of the liquid ligaments and spray.

It is obvious that this phenomena would be very detrimental to stable engine operation because the injection mixing explosions are triggering sources for spray detonation as seen in the more severe "pops." Also the severe "pop" causes flow transients as shown in Figure 24 which is a complete history of the spray detonation "pop." The propellant flows are shutoff for several milliseconds which in itself is detrimental to smooth engine operation.

To get a feel for the pressure field around the injection mixing explosion, a pressure decay calculation was made. The explosion pressure was calculated by assuming that all of the liquid propellant within the ligament breakup region burns to completion within that volume and then expands isentropically. The results plotted in Figure 25 show that the pressure felt by the injector face is very high, whereas the pressure at a 1.0 inch radius has decayed to about 300 psi. These results are consistent with the initiation of the previously postulated pop mechanism.

The results of these observations indicate that injection mixing explosions are indeed capable of initiating spray detonations and that the "pop" observed in large engines is likely a spray detonation initiated by an injection mixing explosion.

CONCLUSIONS

The following presents significant conclusions obtained from the experimental and computational work performed during this study:

1) Experiments have shown that cavitation and two-phase flow is present in the injector and orifices during the space start transient. Further experiments (confirmed by theoretical analysis) show that a discharge coefficient based on cavitational flow does not differ significantly from a discharge coefficient based on noncavitational flow. However, the effect of cavitation will be included as a variable bulk modulus in the transient flow equations and the percentage vapor, due to the cavitation, must be accounted for as input vapor flow.
2) The solution to the system of finite difference equations used to model the vaporization process has been found to be affected by the size of the time step used. The time step size appears to be particularly important during the initial phases of the chamber pressurization. Also, the chamber gas temperature is more noticeably affected than is the chamber pressure.
3) It was shown that changing from a three to a one drop distribution had very little effect on chamber pressurization, even during the initial stages of pressurization. This appears to be true because the solution is the result of sensible heat input rather than vaporization kinetics. The drop radius used for the one drop distribution was the central drop radius of the three drop distribution.
4) Detonation pressure levels are influenced by fuel temperature and subsequent preignition reaction mechanism. For sample times exceeding 2 ms the detonation pressures decrease as the fuel temperature increases (between 500 and 580^{o}R). Detonation pressures were uninfluenced by the wall temperature (between 500 and 580^{o}R) and no trend was observed with oxidizer temperature (between 500 and 580^{o}R).

5) For all propellant lead conditions, the detonation pressures are greater as the delay time to the detonation is increased.

6) Based on the available data it is concluded that large engine "popping" is a detonation wave oriented such that it is damped out, whereas, an undamped wave would grow into a steady-state instability wave. The detonation wave is triggered by low amplitude pressure waves generated by injection mixing explosions.

APPENDICES

APPENDIX A - TRANSIENT PRESSURE HISTORY PROGRAM

APPENDIX B - SUPPLEMENTAL EQUATIONS FOR TRANSIENT PROPELLANT FLOW

```
      PROGRAM PRESS(INPUT,OUTPUT,TAPE 5=INPUT,TAPE 6=OUTPUT)
C          TRANSIENT PRESSURE HISTORY PROGRAM
C
      COMMON /A/       IFP(2),TAU(2),TAUF(2),TAUS(2),XM(2),GAM(2),TG(2),
     1PG(2),      M(2),GEVAP(2),X1(2),XR(2)  ,     ROL(2),CPL(2),TO(2)
      COMMON /ABCDEF/X(1000,2),T(1000,2),P(1000,2),R(1000,2)
      DIMENSION PLANK(2),PCPV(2),PVV(2),CONST7(2),YREACT(10,2)
      DIMENSION TTABLE(10),A(12,10,2),EACTT(10),YK(20,2),PCT(20,2),
     1PTAN(20,2),TP(20,2),AAT(10)
      DIMENSION PV(10), TD(10),TAG(2),PVW(2),PVF(4),TDK(4)
      DIMENSION W1(20,2),T1(20,2),W(1000,2)
      DIMENSION TA(4),CPLA(4),G(2),GCOND(2),XMNOZ(2),TQ(2)
      DIMENSION PG1(2),XMMM(2),RR2(2)
      DIMENSION ROP(2)
      DIMENSION VDROP(2),XMU(2),CPG(2),XK(2),HC(3,2)       ,REACT(2),RE(2
     1),PR(2),H(2),Z(2),QBIG(2),PHE(2),PROD(10)
      DIMENSION WTOTAL(2),GAN(2),CVG(2),EPCOE(2),WDROP(2),F(2)
      DATA (ROP(1)=89.93),(ROP(2)=56.32)
      DATA ((PV(I),I=1,9)=389.29,720.,1324.8,2128.32,2733.12,4419.36,
     15561.28,6946.56,10673.28)
      DATA ((TD(I),I=1,9)=471.84,490.,510.,530.,540.,560.,570.,580.,610.
     1)
      DATA ((PVF(I),I=1,4)=79.2,300.96,720.,1051.2)
      DATA ((TDK(I),I=1,4)=474.,528.,564.,582.)
      DATA ((CPLA(I),I=1,4)=.3667,.3696,.3752,.4168)
      DATA ((TA(I),I=1,4)=524.8,530.,540.,600.)
      NAMELIST/OUT/QBIG,REO,PG,TQ,C1,C2,DENOM,XMNOZ,I,J,N,L,GCOND
      NAMELIST /INPUT/ NN,M,NSTOP,    VDROP,XMU,CPG,XK,XMP,CPGP,AA,RN,
     1RM,EACT,GAMP,HREACT,HC,A,TFP,TAUS,TAUF,XM,GAM,TG,PG,PVW,ASTAR,
     2VC,AC,ALPHA,DELTN,XR,RC,TTABLE,EACTT,YREACT,YK,PCT,PTAN,TP
     3,TW
      CALL SECOND(EXTIME)
      WRITE(6,4444) EXTIME
 4444 FORMAT(1H0,30X,*TIME IS*,F12.3)
    1 READ(5,9000) NN,M(1),M(2),NTRAN,TMAX,DTMIN,DTMAX,CFORPR
      NSTOP=520
      DO 2 L=1,2
      DO 2 I=1,NSTOP
      X(I,L)=0.
      T(I,L)=0.
      P(I,L)=0.
    2 R(I,L)=0.
      DO 6 I=1,10
    6 PROD(I)=0.
      READ(5,9005) VDROP(1),VDROP(2),XMU(1),XMU(2),CPG(1),CPG(2),XK(1),X
     1K(2),XMP,CPGP,RM,RN,XR(1),XR(2),GAMP,TW,CVG(1),CVG(2)
      READ(5,9005) W(1,1),W(1,2),TFP(1),TFP(2),TAUF(1),
     1TAUF(2),TAUS(1),TAUS(2),XM(1),XM(2),GAM(1),GAM(2),TG(1),TG(2),
     2PG(1),PG(2),PVW(1),PVW(2),ASTAR,VC,AC,ALPHA,DELTN
      READ(5,9005)((HC(I,J),I=1,3),J=1,2)
      READ(5,9010) R(1,1),R(1,2),T(1,1),T(1,2)
C
      READ(5,9005)((A(J,I,1),J=1,12),I=1,NN)
      READ(5,9005)((A(J,I,2),J=1,12),I=1,NN)
      READ(5,9005)(EACTT(I),I=1,NN)
      NN1=NN+1
      READ(5,9005)(TTABLE(I),I=1,NN1)
```

```
      READ(5,9005) (YREACT(I,1),I=1,NN)
      READ(5,9005) (YREACT(I,2),I=1,NN)
      READ(5,9005) (YK(I,1),I=1,NTRAN)
      READ(5,9005) (YK(I,2),I=1,NTRAN)
      READ(5,9005) (PCI(I,1),I=1,NTRAN)
      READ(5,9005) (PCI(I,2),I=1,NTRAN)
      READ(5,9005) (PTAN(I,1),I=1,NTRAN)
      READ(5,9005) (PTAN(I,2),I=1,NTRAN)
      READ(5,9005) (TP(I,1),I=1,NTRAN)
      READ(5,9005) (TP(I,2),I=1,NTRAN)
      READ(5,9005) (AA1(I),I=1,NN)
 9000 FORMAT(4I6,4E12.8)
 9005 FORMAT(6E12.8)
 9010 FORMAT(4E12.8)
C          COMPUTE INITIAL CONDITIONS
      DO 15 K=1,8
      IF(T(1,1) .GE. TD(K) .AND. T(1,1) .LE. TD(K+1)) GO TO 10
   15 CONTINUE
   10 PVV(1)=(PV(K)-PV(K+1))*(TD(K+1)-T(1,1))/(TD(K+1)-TD(K))+PV(K+1)
      COE=T(1,2)/1.8-45.46
      COEF=7.8068/-168.*/COE
      PVV(2)=2.935*10.**COEF
      RR2(1)=R(1,1)**3
      RR2(2)=R(1,2)**3
      IF(XM(1) .GT. 0.) XMMM(1)=SQRT(XM(1))
      IF(XM(2) .GT. 0.) XMMM(2)=SQRT(XM(2))
           RC = 1545.
      GEVAP1=0.
      GEVAP2=0.
      REACT(1)=0.
      REACT(2)=0.
      DT1000=1000.*DELTIN
      PPN=0.
      XMNO7P=0.
      GCOND(1)=0.
      GCOND(2)=0.
      TRUE=0.
      INDICA=0.
       GCONDP=0.
      TG(1)=T(1,1)
      TG(2)=T(1,2)
      WRITE(6,INPUT)
      TGP=TG(1)
      TQP=TGP
      TFINAL=1.
      PGTOTAL=0.
      DENOMP=0.
      PGTOTL=0.
      WTOTAL(1)=0.
      WTOTAL(2)=0.
      WDROP(1)=0.
      WDROP(2)=0.
      XMNO7(1)=0.
      XMNO7(2)=0.
      IFIRST=0
      PGP=0.
           CONST1= 4.*ALPHA*       3.1415/SQRT(6.2831853*RC/32.2)
           CONST2= 3.*ALPHA/       SQRT(6.2831853*RC/32.2)
```

```
      CONST3= CONST2*AC/3.
      CONST4 = ASTAR*SQRT(32.2/1545.)
     CONST5=SQRT((32.2*XMP/RC)*(2./(GAMP+1.))**((GAMP+1.)/(GAMP-1.)))*
     1       ASTAR
      PAGE=1
C
      TIME1=DELTN
      TIME=DELTN*1000.
      N22=NOW-1
      NSTOP = NSTOP+1
      TAG(1)=0.
      TAG(2)=0.
C
C          SELECT THE CORRECT PROBLEM
C
          NPP = 0
          NPF =
          IF(M(1).EQ.0) NPF = 2
          IF(M(2).EQ.0) NPF = 1
          IF(NPF .EQ. 0) NPF=3
          IF(M(1).EQ.M(2)) NPF =4
          IF((M(1).LE.M(2)).AND.(M(1).GE.1))      N=1
          IF((M(2).LE.M(1)).AND.(M(2).GE.1))      N=2
       IF(NPF.LT.3) N=NPF
C
C          THE TIME LOOP
C
      L=0
   25 L=L+1
      GEVAP2=GEVAP1
      QBIG(1)=0.
      QBIG(2)=0.
      TAG(N)=0.
            GEVAP(1) =0.
            GEVAP(2) =0.
               X1(1) =0.
               X1(2) =0.
      LX=L
       IF(NPF.NE.4) GO TO 205
   50 N=1
      TAG(N)=0.
       LX=L-M(1)+1
      IF((LX.GE.1).AND.(M(1).GT.0)) GO TO 205
  100 N=2
      TAG(N)=0.
      LX=L-M(2)+1
      IF((LX.GE.1).AND.(M(2).GT.0)) GO TO 205
      GO TO 800
  205 BB=XMMM(N)
      CC=W(LX,N)
      DO 700 NNN=1,LX
      J=LX-NNN+1
      TT=T(J,N)
      RR=R(J,N)
      XX=X(J,N)
       IF(N.EQ.1) GO TO 250
      COE=TT/1.8-45.46
      COEF=7.80687-1680.745/COE
```

```
      PP=2.985*1 .**COEF
      P(J,N)=PP
      TAU(2)=667.
      ROL(2)=62.4*1.253*(1.-.00085*(COE-227.74))
       PL(2)=.75
            GO TO 31
C
C
C
  250 .    CONTINUE
      DO 260 K=1,8
      IF(TT .GE. TD(K) .AND. TT .LE. TD(K+1)) GO TO 270
  260 CONTINUE
      WRITE(6,261)
  261 FORMAT(1H0,2X,84HVAPOR PRESSURE CANNOT BE COMPUTED BECAUSE THE TEM
     1PERATURE IS NOT IN THE PROPER RANGE)
  270 PP= (PV(K)-PV(K+1))*(TD(K+1)-TT)/(TD(K+1)-TD(K))+PV(K+1)
      P(J,1)=PP
      GO TO 290
  280 TAU(1)=178.
      IF(TT .LT. 140.4) ROL(1)=122.49
      IF(TT .GE. 140.5 .AND. TT .LT. 471.84) ROL(1)=-.08433*TT+134.33
      IF(TT .GE. 471.84) ROL(1)=-.0793*TT+131.98
      IF(TT .GE. 524.8) GO TO 300
      IF(TT .GE. 471.84 .AND. TT .LT. 524.8) CPL(1)=.0002325*TT+.2446
      IF(TT .GE. 105.91 .AND. TT .LT. 471.84) CPL(1)=.0004909*TT+.0569
      IF(TT .LT. 105.91) CPL(1)=.00125*TT-.02349
      GO TO 310
  300 DO 305 K=1,3
      IF(TT .GE. TA(K) .AND. TT .LE. TA(K+1)) GO TO 307
  305 CONTINUE
      WRITE(6,306)
  306 FORMAT(1H0,2X,75HCPL(1) CANNOT BE COMPUTED BECAUSE THE TEMPERATURE
     1 IS NOT IN THE PROPER RANGE)
  307 CPL(1)=(CPLA(K)-CPLA(K+1))*(TA(K+1)-TT)/(TA(K+1)-TA(K))+CPLA(K+1)
  310  CONTINUE
      IF(XX .GE. 1.) GO TO 312
      G(N)= ((PP-PG(N))*RR**2/SQRT(TT))*CONST1*BB*DELTN
        IF(G(N).LT.0.) G(N)=0.
       GO TO 316
  312 G(N)=0.
  316 TOG=(G(N)*CG*XR(N)/(ROL(N)*RR2(N)))*.2387
       GEVAP(N) = GEVAP(N)+ TOG
      TAG(N)=TAG(N)+TOG*TT
      IF(XX .GE. 1.) X(J+1,N)=1.
      IF(PP .LE. PG(N)) GO TO 315
      IF(XX .GE. 1.) GO TO 315
      R(J+1,N)=RR*(1.-BB*(PP-PG(N))*DELTN*CONST2/(ROL(N)*SQRT(TT)
     1*RR))**.3333
      GO TO 320
  315 R(J+1,N)=RR
  320 RE(N)=2.*RR*VDROP(N)*XM(N)*PG(N)/(XMU(N)*RC*TG(N))
      PR(N)= CPG(N)*XMU(N)/XK(N)
      PRO = PR(N)**.33333
      REO = RE(N)**.5
       H(N) = XK(N)*(2.+.6*PRO*REO)/(2.*RR)
      Z(N) = G(N)*CPG(N)/(12.566*H(N)*DELTN*RR**2)
      IF(Z(N) .GT. 30.) Z(N)=30.
```

```
      IF(Z(N) .LT. 1.E-10) GO TO 325
      Z(N) = Z(N)/(2.71828**Z(N)-1.)
      GO TO 326
  325 Z(N)=1.
  326 PHE(N)=3.*H(N)*(TG(N)-TT)*RR**2                *Z(N)*DELTN/(ROL(N)*
     1CPL(N)*RR**3)
      QBIG(N)=QBIG(N)+3.*H(N)*RR**2        *Z(N)*DELTN*(TG(N)-TT)*
     1XR(N)*CC        /(RR2(N)*ROL(N))
      IF(XX .GE. 1.) GO TO 360
      IF(PP .GT. PG(N)) GO TO 340
      T(J+1,N)=TT
      IF(T(J+1,N) .LE. TFP(N)) GO TO 350
      GO TO 370
  340 T(J+1,N)=  II        -CONST2*DELTN*TAU(N)*(PP-PG(N))/(ROL(N)
     1*CPL(N)*RR       *SQRT(TT) )      *BB+PHE(N)
      IF(T(J+1,N) .LT. TFP(N)) T(J+1,N)=TFP(N)
      IF(T(J+1,N) .GT. TFP(N)) GO TO 370
  350 X(J+1,N)=XX             + (G(N)*TAUS(N)/(ROL(N)*       RR**3*TAUF(N)))
     1*.2387-CPL(N)*PHE(N)/TAU(N)
       GO TO 370
  360 T(J+1,N)=TFP(N)
  370                              CONTINUE
  700      CONTINUE
      PPG=PG(N)
      IF(NPF .EQ. 4) PPG=PGTOTL
      DO 2500 K1=1,NTRAN
      IF(PPG .GE. PCT(K1,N) .AND. PPG .LE. PCT(K1+1,N)) GO TO 2507
      K1=K1
 2500 CONTINUE
 2507 CONST7(N)=(YK(K1+1,N)-YK(K1,N))*(PCT(K1+1,N)-PPG)/(PCT(K1,N)
     1-PCT(K1+1,N))+YK(K1+1,N)
      DO 2600 K=1,NTRAN
      IF(TIME1.GE. TP(K,N) .AND. TIME1.LE. TP(K+1,N)) GO TO 2607
      K=K
 2600 CONTINUE
 2607 PTANK(N)=(PTAN(K+1,N)-PTAN(K,N))*(TP(K+1,N)-TIME1)/(TP(K,N)
     1-TP(K+1,N))+PTAN(K+1,N)
      PCPV(N)= PG(N)
      IF(PG(N) .LE. PVV(N)) PCPV(N)=PVV(N)
           IF(NPF.EQ.1) GO TO 800
           IF(NPF.EQ.2) GO TO 800
           IF(NPF.EQ.3) GO TO 710
          IF((NPF.EQ.4).AND.(N.EQ.2)) GO TO 800
           IF((NPF.EQ.4).AND.(N.EQ.1)) GO TO 100
  710      IF(N.EQ.1) MPF=2
           IF(N.EQ.2) MPF=1
           IF(M(MPF).EQ.L) NPF=4
           IF(NPF.NE.4) GO TO 800
      IF(MPF.EQ.2) GO TO 100
      IF(MPF.EQ.1) GO TO 50
  800      CONTINUE
C
           IF(NPF.EQ.4) N=1
  810  GCOND(N)=((PG(N)-PVW(N))*CONST3*DELTN/SQRT(TG(N)))*BB
       IF(GCOND(N).LT.0.) GCOND(N)=0.
      LX=L-M(N)+1
      WTOTAL(N)=WTOTAL(N)+W(LX,N)-XMNOZ(N)-REACT(N)
      TO(N)=WTOTAL(N)
```

```
      WDROP(N)=W(LX,N)   -GCOND(N)-GEVAP(N)+WDROP(N)
      F(N)=WDROP(N)/WTOTAL(N)
       XMNOZ(N) = (PG(N)/SQRT(TG(N)))*CONST4*BB*SQRT(GAM(N)*(2./(GAM(N)+
     11.)))**((GAM(N)+1.)/(GAM(N)-1.)))
       XMNOZ(N)=XMNOZ(N)*DELTN
       DENOM=GEVAP(N)+VC*XM(N)*PG(N)/(RC*TG(N))-GCOND(N)-XMNOZ(N)
        1(N)=DENOM
       C1=0.
       C2=0.
       IF(PG(N) .LT. 44.) GO TO 4
       IF(TW.GT.TG(N)) GO TO 3
       C2=HC(2,N)*AC*(TG(N)-TW)*DELTN/CPG(N)
       C1=0.
       GO TO 4
     3 C1=HC(1,N)*AC*(TW-TG(N))*DELTN/CPG(N)
       C2=0.
     4 TQ(N)=(TAG(N)+VC*XM(N)*PG(N)/RC-(GCOND(N)+XMNOZ(N))*TG(N)+C1-C2)/
      1DENOM
C
       PG(N)=GEVAP(N)*RC*TQ(N)/(VC*XM(N))-RC*TQ(N)*GCOND(N)/(VC*XM(N))
      1-RC*TQ(N)*XMNOZ(N)/(VC*XM(N))+PG(N)*TQ(N)/TG(N)
        PG1(N)=PG(N)/144.
       W(LX+1,N)=CONST7(N)*SQRT((PTANK(N)-PCPV(N))*.367)*DELTN
C
            IF(NPF.NE.4) GO TO 820
       IF((NPF.EQ.4) .AND. (N.EQ.2)) GO TO 1100
            N=2
            GO TO 810
  815 PGTOTL=PG1(1)+PG1(2)
            GO TO 825
  820 PGTOTL=PG(N)
  825 IF(NPAGE .EQ. 1) WRITE(6,2000)
       IF(NPF .EQ. 4) GO TO 900
       IF(N .EQ. 1) GO TO 920
        RITE(6,2030) TIME,PG1(2),GEVAP(2),GCOND(2),TG(2),WTOTAL(2),F(2)
       NPAGE=NPAGE+1
       IF(NPAGE.GE.60) NPAGE=1
       GO TO 990
  920 WRITE(6,2030) TIME,PG1(1),GEVAP(1),GCOND(1),TG(1),WTOTAL(1),F(1)
       NPAGE=NPAGE+1
       IF(NPAGE.GE.60) NPAGE=1
       GO TO 990
  900 WRITE(6,2030)  TIME,PG1(1),PG1(2),GEVAP(1),GEVAP(2),GCOND(1),GCOND
     1(2),TG(1),TG(2)
       NPAGE=NPAGE+1
       IF(NPAGE.GE.60) NPAGE=1
  990 CONTINUE
 2000 FORMAT(1H1,4X,4HTIME,9X,2HPG,12X,5HGEVAP,9X,5HGCOND,9X,2HTG,12X,6H
     2WTOTAL,8X,2HF )
     1P(2),5X,8HGCOND(1),5X,8HGCOND(2),5X,5HTG(1),8X,5HTG(2))
 2010 FORMAT(1H ,E13.4,13X,E13.4,13X,E13.4,13X,E13.4,13X,E13.4)
 2020 FORMAT(1H ,E13.4,E13.4,13X,E13.4,13X,E13.4,13X,E13.4,E13.4)
 2030 FORMAT(1H ,9E13.4)
 3000   CONTINUE
       TG(N)=TQ(N)
       LLLLLL=L+1
       IF((NPF .EQ. 3) .AND. (M(MPF) .EQ. LLLLLL)) NPF=4
        GO TO 115
```

```
 1100 CONTINUE
C
C
C
      TAVERG=(PG(1)*XM(1)*CPG(1)+PG(2)*XM(2)*CPG(2)+PGP*XMP*CPGP)/(PG(1)
     1*XM(1)*CPG(1)/TQ(1)+PG(2)*XM(2)*CPG(2)/TQ(2)+PGP*XMP*CPGP/TFINAL)
     2-(QBTG(1)+QBTG(2))/(X1(1)*CPG(1)+X1(2)*CPG(2)+DENOMP*CPGP)
C
C
C
      CON=PG(1)*VC/(RC*TQ(1))
      CFN=PG(2)*VC/(RC*TQ(2))
      DO 1105 K=1,NN
      IF(TAVERG .GE. TTABLE(K) .AND. TAVERG .LE. TTABLE(K+1)) GO TO 1107
      K=K
 1105 CONTINUE
 1107 AA=AAT(K)
      EACT=EACTT(K)
      K3=1
      IF(CON/CFN .GT. CFORPR) K3=2
      YREACT=YREACT(K,K3)
      REACT(1)=VC*AA*XM(1)*(CON/VC)**RN*(CFN/VC)**RM*2.71828**(-EACT/
     1(RC*TAVERG))*DELTN
      RPN=0.
      C1=0.
       2=0.
      IF(REACT(1) .GT. CON*XM(1)) REACT(1)=CON*XM(1)
      REACT(2)=A(2,K,K3)*REACT(1)/A(1,K,K3)
      IF(REACT(2) .LT. CFN*XM(2)) GO TO 1110
      REACT(2)=CFN*XM(2)
      REACT(1)=A(1,K,K3)*REACT(2)/A(2,K,K3)
 1110 DO 1120 I=1,10
      DPRN=REACT(1)*A(I+2,K,K3)/A(1,K,K3)
      IF(I .GT. 8) GO TO 1120
      RPN=RPN+DPRN
 1120 PROD(I)=PROD(I)+DPRN
      DENOMR=(X1(1)-REACT(1))*CPG(1)+(X1(2)-REACT(2))*CPG(2)+DENOMP*CPGP
      DELTRE=REACT(1)*HREACT/DENOMR
      TFINAL=TAVERG+DELTRE
      DO 1130 NX=1,2
      PG(NX)=PG(NX)*TFINAL/TQ(NX)
      PG(NX)=PG(NX)-REACT(NX)*RC*TFINAL/(XM(NX)*VC)
      IF(PG(NX) .LT. 0.) PG(NX)=0.
      PG1(NX)=PG(NX)/144.
 1130 CONTINUE
      PGP=TFINAL*(RPN*RC/(VC*XMP)-RC*XMNOZP/(VC*XMP)+PGP/TGP)
      XMNOZP=(PGP*ASTAR*DELTN/SQRT(TFINAL))*CONST5*DELTN
      DENOMP = RPN+VC*XMP*PGP/(RC*TGP)-XMNOZP
      IF(PGP .LT. 144.) GO TO 1140
      IF(TW.GT.TGP) GO TO 1135
      C1=0.
      C2=HC(3,2)*AC*(TGP-TW)*DELTN/CPGP
      GO TO 114
 1135 C2=0.
      C1=HC(3,1)*AC*(TW-TGP)*DELTN/CPGP
 1140 TQP = (RPN*TGP+VC*XMP*PGP/RC     -XMNOZP*TGP-C2+C1)/DENOMP
      TG(1)=TFINAL
      TG(2)=TFINAL
```

```
      TGP    =TFINAL
      PGP1=PGP/144.
      PGTOTAL=PGP1+PG1(1)+PG1(2)
      PGTOTL=PG(1)+PG(2)+PGP
      IF(PGTOTAL .GE. 10.) GO TO 1
 2001 FORMAT(1H1,4X,4HTIME,10X,12HPG(1)/PRD(3),2X,12HPG(2)/PRD(4),2X,12H
     1PGTOL/PRD(5),2X,10HPGP/PRD(6),4X,14HREACT1/PRD(7) ,14HREACT2/PRD(8
     2) ,14HPRD(1)/PRD(9) ,14HPRD(2)/PRD(10),/,19X,6HTFINAL,8X,6HTAVERG,
     38X,6HDELTRE,8X,9HWTOTAL(1),5X,9HWTOTAL(2),5X,4HF(1),10X,4HF(2),10X
     4,2HTQP)
 2031 FORMAT(1H ,9E14.4)
 2032 FORMAT(1H ,14X,8E14.4)
      IF((IFIRST .EQ. 0) .OR. (NPAGE .EQ. 1)) WRITE(6,2001)
      WRITE(6,2031) TIME,PG1(1),PG1(2),PGTOTAL,PGP1,REACT(1),REACT(2),
     1PROD(1),PROD(2)
      WRITE(6,2032)(PROD(I),I=3,10)
      WRITE(6,2032) TFINAL,TAVERG,DELTRE,TO(1) ,  TO(2)   ,F(1),F(2),
     1TQP
      IFIRST=1
      NPAGE=NPAGE+3
      IF(NPAGE .GE. 57) NPAGE=1
 1150 CONTINUE
      TIME=TIME+0.1000
      TIME1=TIME1+DELTN
 1000   CONTINUE
      DELTN=SQRT((TIME+.01)/1.E+10)
      IF(TIME1 .GE. TMAX) GO TO 1
      IF( L .GE. NSTOP) GO TO 1
      DT1000=DELTN*1000.
      GO TO 25
      END
```

APPENDIX B

SUPPLEMENTAL EQUATIONS FOR TRANSIENT PROPELLANT FLOW

The effective velocity of sound in a liquid filled line is determined by:

$$V_s = \frac{12}{\left[\frac{\rho_\ell}{g}\left(\frac{1}{\beta_\ell} + \frac{d}{E_p \ell}\right)\right]^{1/2}} \tag{B-1}$$

The number of wave reflections between the tank and propellant valve during the valve opening time is:

$$N = \frac{V_s t_{vo}}{2L} \quad . \tag{B-2}$$

A wave is reflected at the valve with less intensity than the incident wave when the valve is partially open. This reflection factor is:

$$\Psi_m = \frac{1 - \Phi_n}{1 + \Phi_n} \quad , \tag{B-3}$$

where

$$\Phi_n = \left(\frac{A_v}{A_p}\right)\left(\frac{n}{N}\right) \quad . \tag{B-4}$$

REFERENCES

1. Bell Aerosystems: Agena Vacuum Start Improvement Program, (1965).

2. Knox, R. M.; Minton, S. J.; and Zwick, E. B.: Space Ignition. Paper presented at AIAA 2nd Propulsion Jt. Spec. Conf. (Colorado Springs, Colo.) June, 1966.

3. Clayton, R.M.: The Influence of Several Near-Wall Injection Conditions on the Combustion Performance of a Liquid Rocket Engine. NASA Technical Report 32-1283, Jet Propulsion Laboratory, Pasadena, Calif. (1966).

4. Zung, L.B.; Breen, B.P.; and Kushida, R.: A Basic Study of Ignition of Hypergolic Liquid Propellants. Western States Section/The Combustion Institute Paper No. 68-43 (Oct. 1968), (Available through Dynamic Science).

5. Perlee, Henry E. and Christos, Theodore: Summary of Hypergolic Ignition Spike Phenomena. U.S. Dept. of the Interior, Bureau of Mines, Final Report No. 3982, April 8 to December 31, 1965.

6. Dauerman, L.; Ray, A. B.; Koehler, G.; and Salser, G.E.: Evidence for the Formation of Azides in the N_2H_4/N_2O_4 Reaction. AIAA Journal (Nov. 1968), p. 2186.

7. Agosta, Vito D.; and Graus, George: An Investigation of the Impulse Bit Developed by a Pulsed Liquid Propellant Rocket Engine. Curtiss-Wright Corp. (1964).

8. Seamans, T.F. and Dawson, B.E.: Hypergolic Ignition at Reduced Pressures. Air Force Technical Report AFRPL-TR-67-175, (1967).

9. Nadig, E.Q.; Tkachenko, E.A.; and Breen, B.P.: A Study of Random Wave Phenomena in Hypergolic Propellant Combustion. Dynamic Science Report No. SN-87, under NASA Contract NAS7-467 (1967).

10. Stevens, M.R.; Fisher, H.D.; Weiss, H.G.; and Breen, B. P.: Effect of Additives on the Ignition Delay Time of Hypergolic Propellants. Western States/The Combustion Institute Paper No. 67-22, (April 1967).

11. Weiss, H.G.: A Basic Study of the Nitrogen Tetroxide/ Hydrazine Reaction. Western States Section/The Combustion Institute Paper No. 65-20, (Oct. 1965).

12. Lawver, B. R.; and Breen, B. P.: Hypergolic Stream Impingement Phenomena-Nitrogen Tetroxide/Hydrazine. NASA-CR-72444, parepared under contract NAS7-467, (1968).

13. Rich, Geo. R.: Hydraulic Transients, Second ed., Dover Publications, Inc., (1963).

14. Streeter, Victor L.; and Wylie E. Benjamin: Hydraulic Transients. McGraw-Hill Book Co., Inc. (1967).

15. Skinner, B. G.; Hedley, W. H.; and Snyder, A.D.: Mechanism and Chemical Inhibition of the Hydrazine-Nitrogen Tetroxide Reaction. (ASD-TDR-62-1041), Monsanto Research Corporation (1962).

16. Zeleznik, Frank J.; and Gordon, Sanford: A General IBM 704 or 7090 Computer Program for Computation of Chemical Equilibrium Compositions, Rocket Performance, and Chapman-Jouquet Detonations. NASA TN D-1454, (1962).

17. Zeleznik, Frank J.; and Gordon, Sanford: Calculation of Detonation Properties and Effect of Independent Parameters on Gaseous Detonations. ARS Journal Vol. 32, No. 4 (April 1962), pp 606-615.

18. Burrows, M.C.: Mixing and Reaction Studies of Hydrazine and Nitrogen Tetroxide Using Photographic and Spectral Techniques, NASA TM X-52244 (1966).

19. Clayton, R.M.; and Rogero, R.S.: Experimental Measurements on a Rotating Detonation-Like Wave Observed During Liquid Rocket Resonant Combustion, Jet Propulsion Laboratory, Technical Report 32-788, (1965).

20. Ragland, K. W.; Dabora, E. K.; and Nicholls, J.A.: Shock Induced Heterogeneous Detonations (preprint) WSCI 65-22, Fall Meeting of Western States Section/The Combustion Institute (1965).

21. Dabora, E.K.; Ragland, K.W.; and Nicholls, J.A.: Spray Detonations. 4th ICRPG Combustion Conference, Vol. 1 (1967).

22. Bollinger, L.E.: Formation of Detonation Waves in Combustible Gaseous Mixtures. Paper presented at the Western States Combustion Institute Meeting, Stanford, Univ. (1964).

23. Urtiew, P.A.; and Oppenheim, A. K.: Detonation Ignition Induced by Shock Merging. Eleventh Symposium on Combustion, Combustion Institute, (1967).

24. Bush, C. W.; Laderman, A. J.; and Oppenheim, A. D.: Parametric Study of the Generation of Pressure Waves by a Particle-Fueled Combustion. AIAA 2nd Annual Meeting and Technical Demonstration, Paper 65-357, (July 1965).

RELATED HYPERGOLIC PROPELLANT BIBLIOGRAPHY

25. Howell, Glen, W., ed.: Aerospace Fluid Component Designers' Handbook. Tech. Doc. Rept. No. RPL-TDR-64-25 (AF04(611)-8385, DDC, No. AD 447995) TRW Space Technology Laboratories, (May 1964).

26. Minton, S. J.; and Zwick, E. B.: Hypergolic Combustion Initiated at Low Pressure. Paper presented at the Aviation Space Conference of the American Society of Mechanical Engineers, (Los Angeles, California) (March 1965).

27. Kappl, J. J.; and Knox, R. M.: Altitude Ignition of Hypergolic Bipropellant Rockets. The Marquardt Corporation (1965).

28. Bernard, J. L. J.; and Dufour, J.: 8th International Symposium on Combustion. On the Existence of Detonation Conditions in the Combustion of Some Nitric Acid Propellants, (1960), pp 1074-1084.

29. Martens, R. E.: Investigation of the Hypergolic Ignition Spike Phenomena. Internal Report, Engineering Gechnology Division, McDonnell Aircraft Corp. (1966).

30. Lawver, B. R.; and Kappl, J. J.: Effects of Additives on Altitude Hypergolic Ignition. Paper presented at AIAA 2nd Propulsion Jt. Specialist Conference (Colorado Springs, Colo.), (June 1966).

31. Lawver, B. R. : Effect of Ignition O/F on Spike Pressure Distribution. Interoffice Memo 153-75/49, Marquardt Corp. (May 1966).

32. Friedman, R.; Barnes, W. P.; and Markels, M. Jr: A Study of Explosions Induced by Contact of Hydrazine-Type Fuels with Nitrogen Tetroxide. Tech. Doc. Rept. (ASD-TR-62-685), Atlantic Research Corp., (Sept. 1962).

33. Kliegel, J. R.; et al: C-1 Engine Final Report. TRW Systems, 5380-6005-RU000, (September 1965).

34. Martinez, E. P. : Propellant Feed System Hydraulics in L/M Reaction Control System. Propulsion and Power Division, Manned Spacecraft Center, (Houston, Texas), (1966).

35. Bowling, R. C.; and Rope, R. K.: Dynamic Interaction Analysis and Computer Model LM Reaction Control Propulsion System. Advanced Technology Laboratories, General Electric Company (March 1965)

36. Priem, R. J.; and Heidmann, M. F.: Propellant Vaporization as a Design Criterion for Rocket-Engine Combustion Chambers, NASA TR-67, (1960).

37. Thomas, D. C. : The Thermal Decomposition of Hydrazine. Progress Report No. 9-14, Jet Propulsion Laboratory, (August 1947).

38. Weiss, Richard, R.; and Klopotek, Raymond D.: Experimental Evaluation of the Titan III Transtage Engine Combustion Stability Characteristics. (AFRPL-TR-66-51), (March 1966).

TABLE I

PARAMETRIC STUDIES FOR SPACE START TRANSIENT

Computation Number	Oxidizer Temp. (°R)	Fuel Temp. (°R)	Wall Temp. (°R)	Lead	Lead Time msec
1	540	540	540	0	0
2	540	540	540	Fuel	2
3	540	540	540	Oxid.	2
4	580	540	540	0	0
5	540	580	540	0	0
6	540	500	540	0	0
7	500	540	540	0	0
8	500	500	540	Fuel	3
9	500	500	540	Oxid.	3
10	540	540	580	0	0
11	540	540	500	0	0
12	500	500	540	0	0

TABLE II

RESULTS OF VAPORIZATION AND DETONATION COMPUTATIONS

Run No.	t (ms)	T_{ox} (°R)	T_{fu} (°R)	T_w (°R)	Lead	P_c (psia)	T_c (°R)	O/F	f (N_2O_4)	f (N_2H_4)	Weight N_2O_4 (lb)	Weight N_2H_4 (lb)	Weight $N_2H_5NO_3$ (lb)	Weight NH_4NO_3 (lb)	P_D (psia)	P_p (psia)	T_D (°R)	Ign. (ms)
1	1	540	540	540	o/-	.83	499	1.67	.655	.953	1.38×10^{-4}	8.27×10^{-5}		5.44×10^{-8}	375	201	3285	-
	2					2.12	525	2.15	.710	.945	4.16×10^{-4}	1.94×10^{-4}		6.19×10^{-7}	757	405	3504	
	3					3.00	551	2.23	.766	.946	6.79×10^{-4}	3.03×10^{-4}		2.20×10^{-6}	1139	610	3520	
2	3	540	540	540	2/F	.92	538	.89	.748	.942	1.94×10^{-4}	2.18×10^{-4}	2.27×10^{-9}	1.91×10^{-6}	498	267	3467	5+
	4					2.17	568	1.44	.770	.945	4.76×10^{-4}	3.29×10^{-4}	2.27×10^{-9}	1.45×10^{-6}	984	526	3668	
	5					4.27	717	1.67	.799	.954	7.35×10^{-4}	4.34×10^{-4}	2.27×10^{-9}	3.75×10^{-6}	1367	731	3664	
3	3	540	540	540	2/Ox	2.52	526	5.65	.768	.974	6.31×10^{-4}	1.11×10^{-4}		5.44×10^{-7}	695	378	2728	-
	4					3.26	545	3.99	.804	.972	8.94×10^{-4}	2.22×10^{-4}		2.21×10^{-6}	1160	626	3067	
	5					3.94	553	3.42	.828	.976	1.15×10^{-3}	3.30×10^{-4}		4.64×10^{-6}	1596	859	3211	
4	1	500	500	540	o/-	.46	478	1.30	.716	.983	9.59×10^{-5}	7.40×10^{-5}		9.64×10^{-9}	237	126	3461	-
	2					1.58	496	2.06	.743	.992	3.82×10^{-4}	1.86×10^{-4}		1.52×10^{-7}	717	383	3514	
	3					2.42	505	2.23	.776	.994	6.62×10^{-4}	2.97×10^{-4}		5.62×10^{-7}	1317	706	3382	
5	4	500	500	540	3/F	.66	487	.70	.761	.994	1.65×10^{-4}	2.36×10^{-4}	6.59×10^{-10}	3.59×10^{-8}	552	294	3558	-
	5					1.65	505	1.31	.682	.998	4.56×10^{-4}	3.48×10^{-4}	6.59×10^{-10}	2.47×10^{-7}	1006	538	3675	
	6					2.40	514	1.60	.805	.996	7.33×10^{-4}	4.58×10^{-4}	6.59×10^{-10}	7.47×10^{-7}	2004	1072	3750	
6	4	500	500	540	3/Ox	2.52	586	7.76	.820	.991	8.85×10^{-4}	1.14×10^{-4}		1.58×10^{-7}	821	451	2389	-
	5					2.75	501	5.12	.853	.994	1.16×10^{-3}	2.26×10^{-4}		6.08×10^{-6}	1385	752	2838	
	6					2.83	500	4.23	.879	.996	1.42×10^{-3}	3.36×10^{-4}		1.12×10^{-6}	1944	1060	3038	
7	1	540	540	580	o/-	.81	498	1.66	.655	.954	1.35×10^{-4}	8.16×10^{-5}		5.23×10^{-8}	375	202	3285	3.6
	2					2.18	543	2.14	.710	.945	4.15×10^{-4}	1.93×10^{-4}		7.78×10^{-7}	756	404	3502	
	3					3.24	590	2.23	.776	.954	6.76×10^{-4}	3.01×10^{-4}		3.35×10^{-6}	1145	613	3513	
8	1	540	540	500	o/-	.81	498	1.66	.655	.954	1.35×10^{-4}	8.16×10^{-5}		5.23×10^{-8}	375	202	3285	-
	2					2.06	511	2.15	.708	.943	4.16×10^{-4}	1.94×10^{-4}		5.22×10^{-7}	759	406	3505	
	3					2.84	522	2.24	.763	.941	6.81×10^{-4}	3.04×10^{-4}		1.48×10^{-6}	1129	604	3525	
9	1	580	540	540	o/-	.95	573	1.65	.665	.956	1.41×10^{-4}	8.54×10^{-5}		2.19×10^{-7}	326	174	3487	2.0
	2					4.63	886	1.95	.688	.975	3.81×10^{-4}	1.88×10^{-4}		1.03×10^{-6}	678	363	3468	
	3																	
10	1	500	540	540	o/-	.59	581	1.51	.716	.955	1.17×10^{-4}	7.78×10^{-5}		2.48×10^{-8}	293	156	3488	-
	2					1.72	502	2.16	.749	.943	4.10×10^{-4}	1.90×10^{-4}		2.95×10^{-7}	726	388	3496	
	3					2.55	514	2.29	.783	.940	6.88×10^{-4}	3.01×10^{-4}		1.02×10^{-6}	1196	646	3511	
11	1	540	580	540	o/-	.95	503	1.82	.658	.874	1.56×10^{-4}	8.54×10^{-5}		9.08×10^{-8}	269	143	3435	3.6
	2					2.28	534	2.21	.709	.860	4.34×10^{-4}	1.96×10^{-4}		9.35×10^{-7}	606	324	3467	
	3					3.30	581	2.27	.776	.869	6.95×10^{-4}	3.03×10^{-4}		3.62×10^{-6}	890	477	3482	
12	1	540	500	540	o/-	.66	495	1.46	.651	.985	1.14×10^{-4}	7.81×10^{-5}		2.07×10^{-8}	322	172	3499	-
	2					1.93	517	2.07	.831	.993	3.96×10^{-4}	1.91×10^{-4}		3.22×10^{-7}	886	474	3538	
	3					2.73	528	2.19	.762	.998	6.62×10^{-4}	3.02×10^{-4}		1.03×10^{-6}	1431	766	3560	

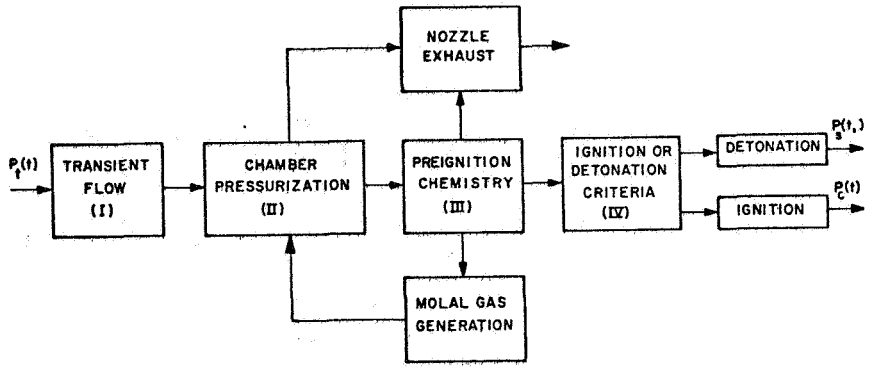

a. Rocket Chamber Ignition

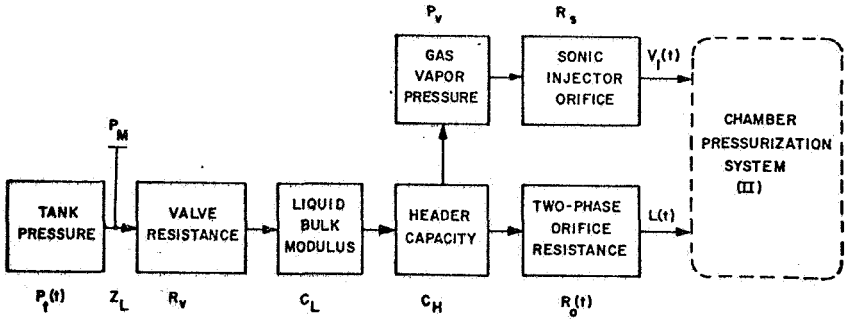

b. Transient Flow Systems (I)

Figure 1. Schematic Diagram of Transient Ignition Model

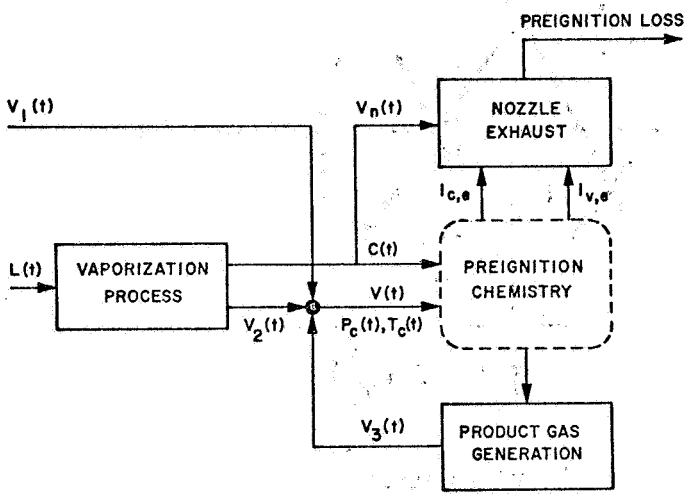

a. Chamber Pressurization System (II)

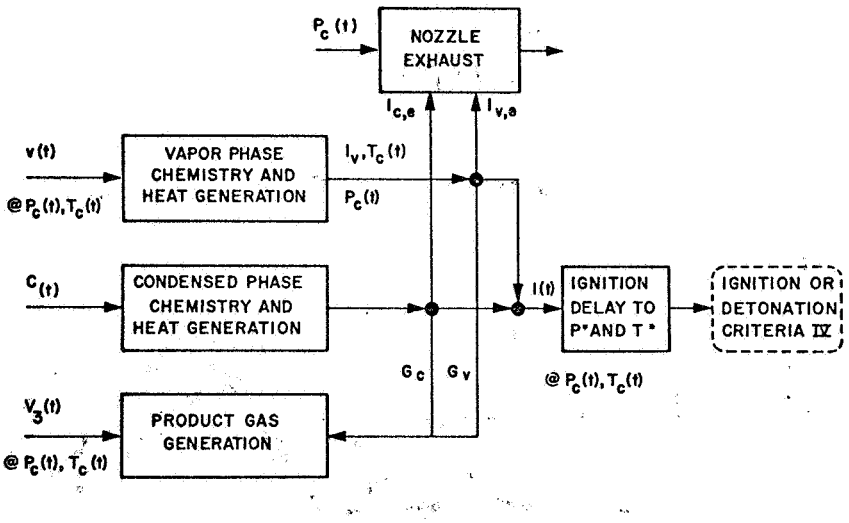

b. Preignition Chemistry System (III)

Figure 2. Schematic Diagram of Transient Ignition Model Systems

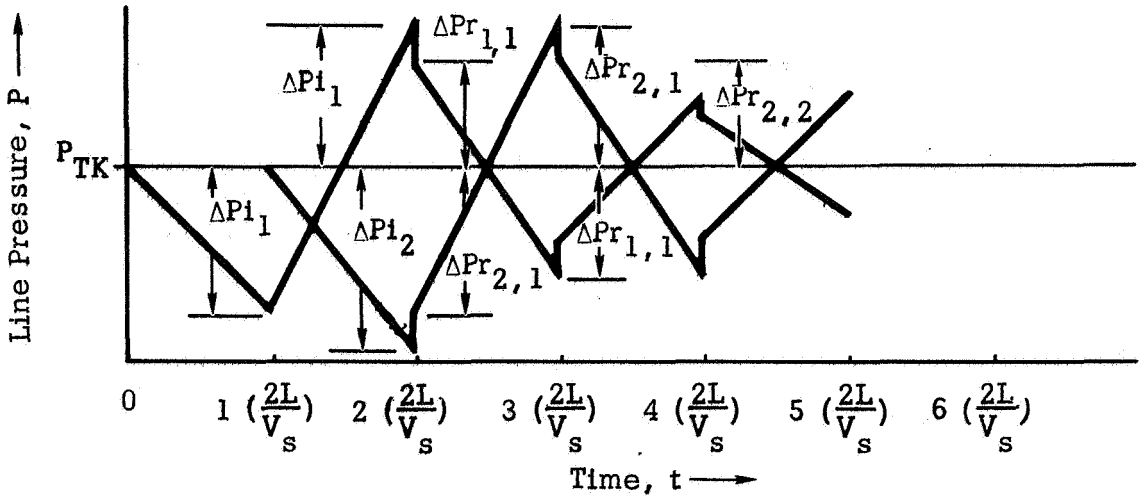

a. Identification of Pressure Surges

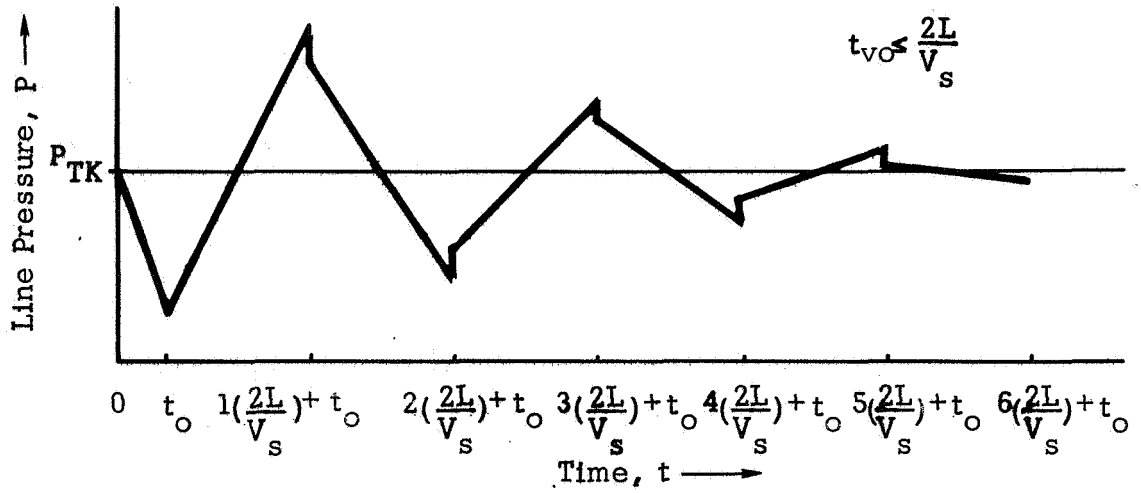

b. Pressure Surge for Quick Valve Opening

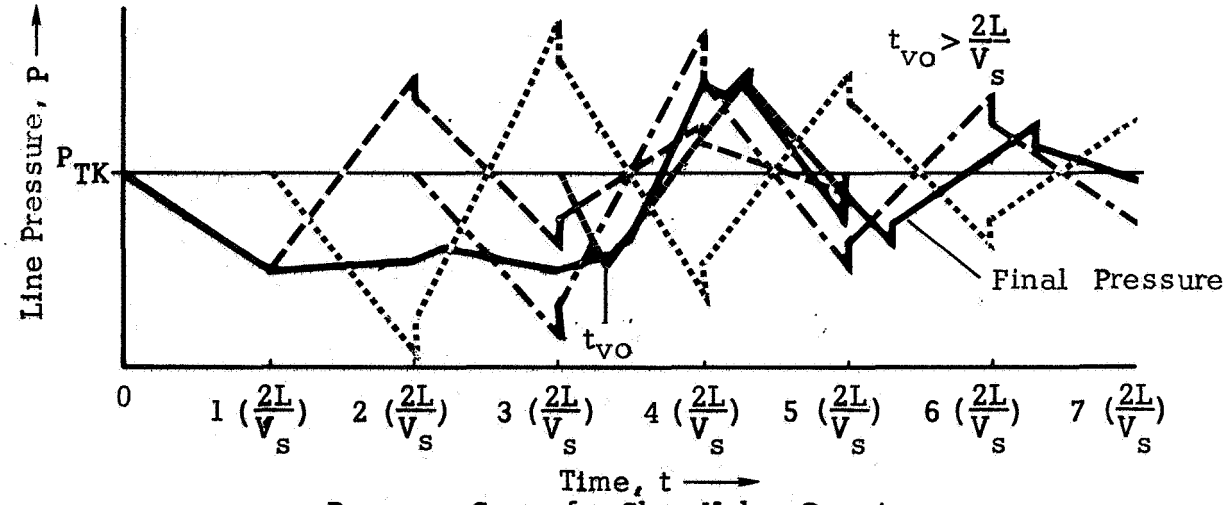

c. Pressure Surge for Slow Valve Opening

Figure 3. Pressure Transients Between Propellant Valve And Tank Caused By Valve Opening

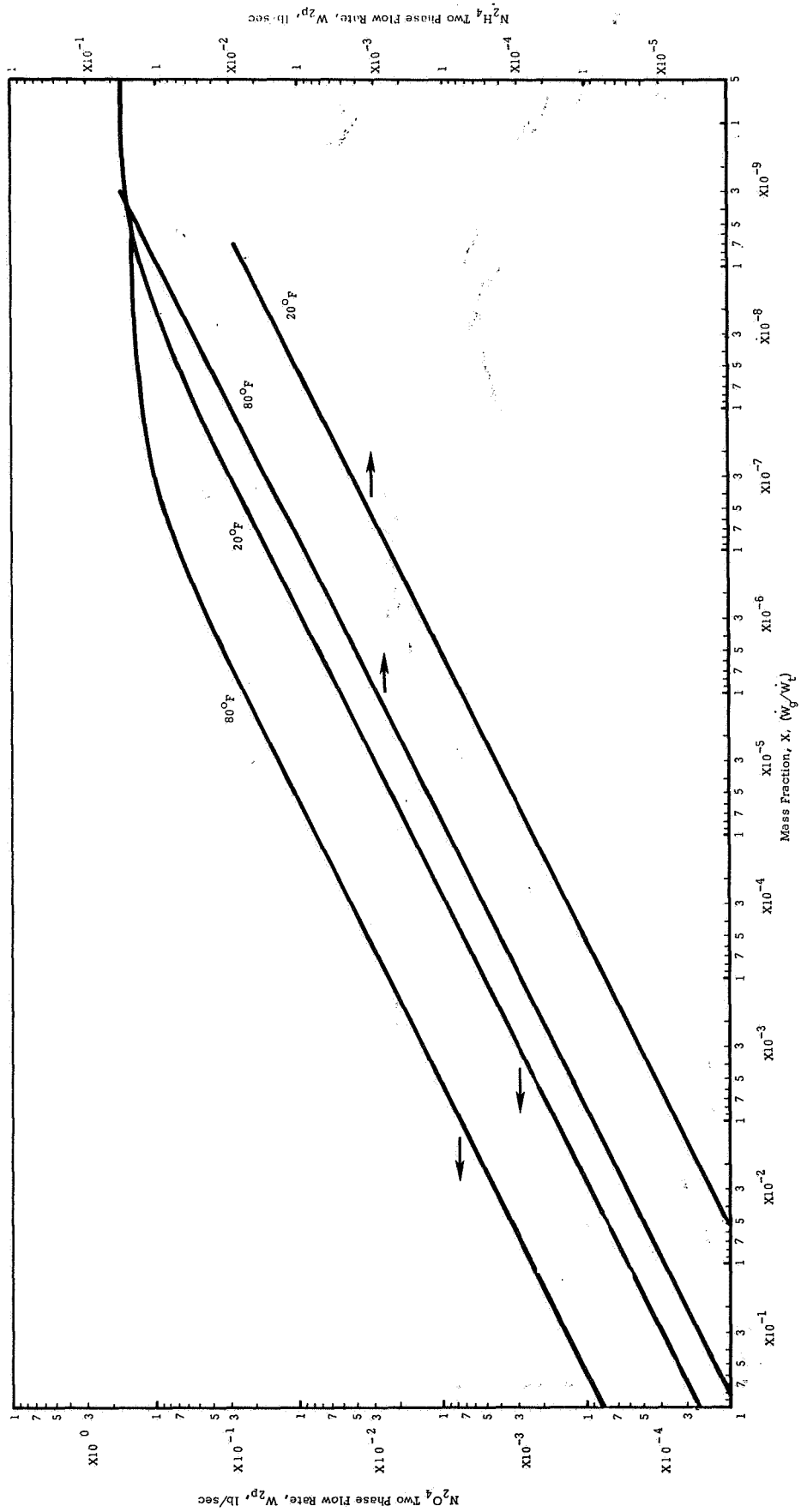

Figure 4. Two-Phase Propellant Flow Rate for N_2H_4 and N_2O_4 Systems at Their Vapor Pressure for Various Mass Fraction Ratios (Assuming Acoustic Velocity and Orifice Diameter = 0.030 in.)

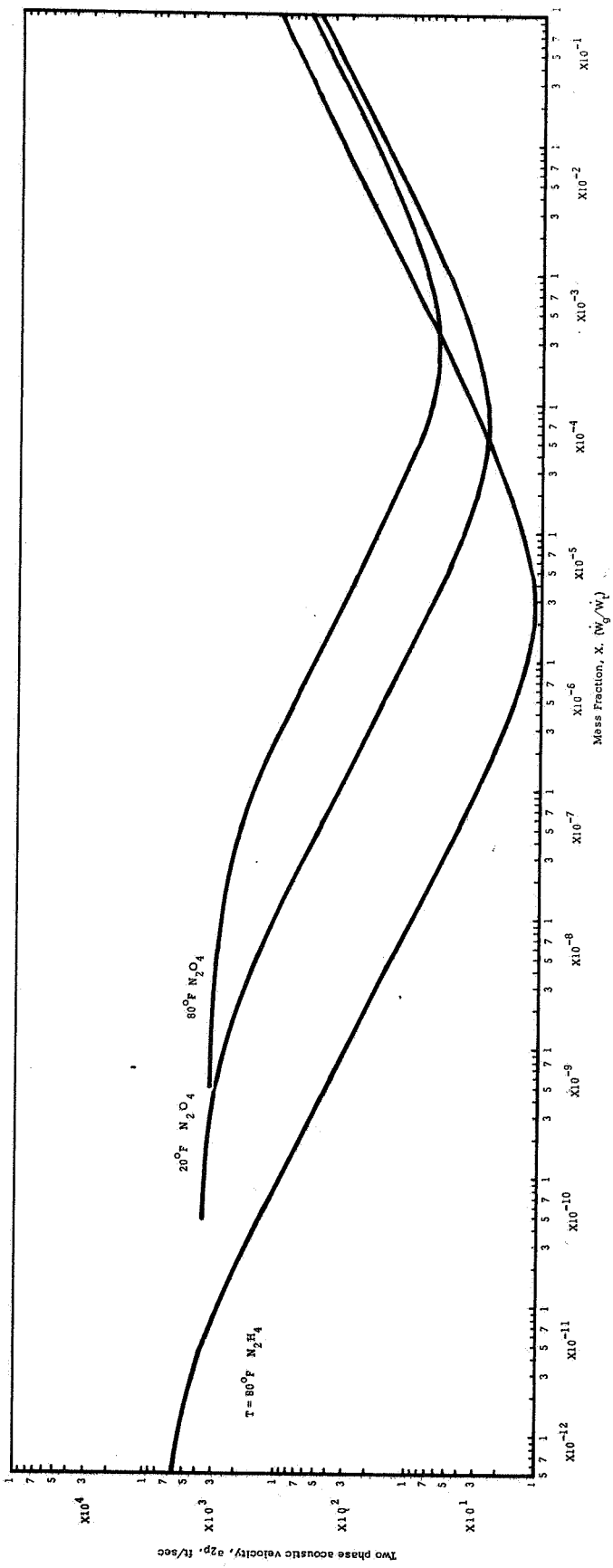

Figure 5. Acoustic Velocity for N_2H_4 and N_2O_4 Liquid-Vapor Systems at Their Vapor Pressure for Various Mass Fraction Ratios.

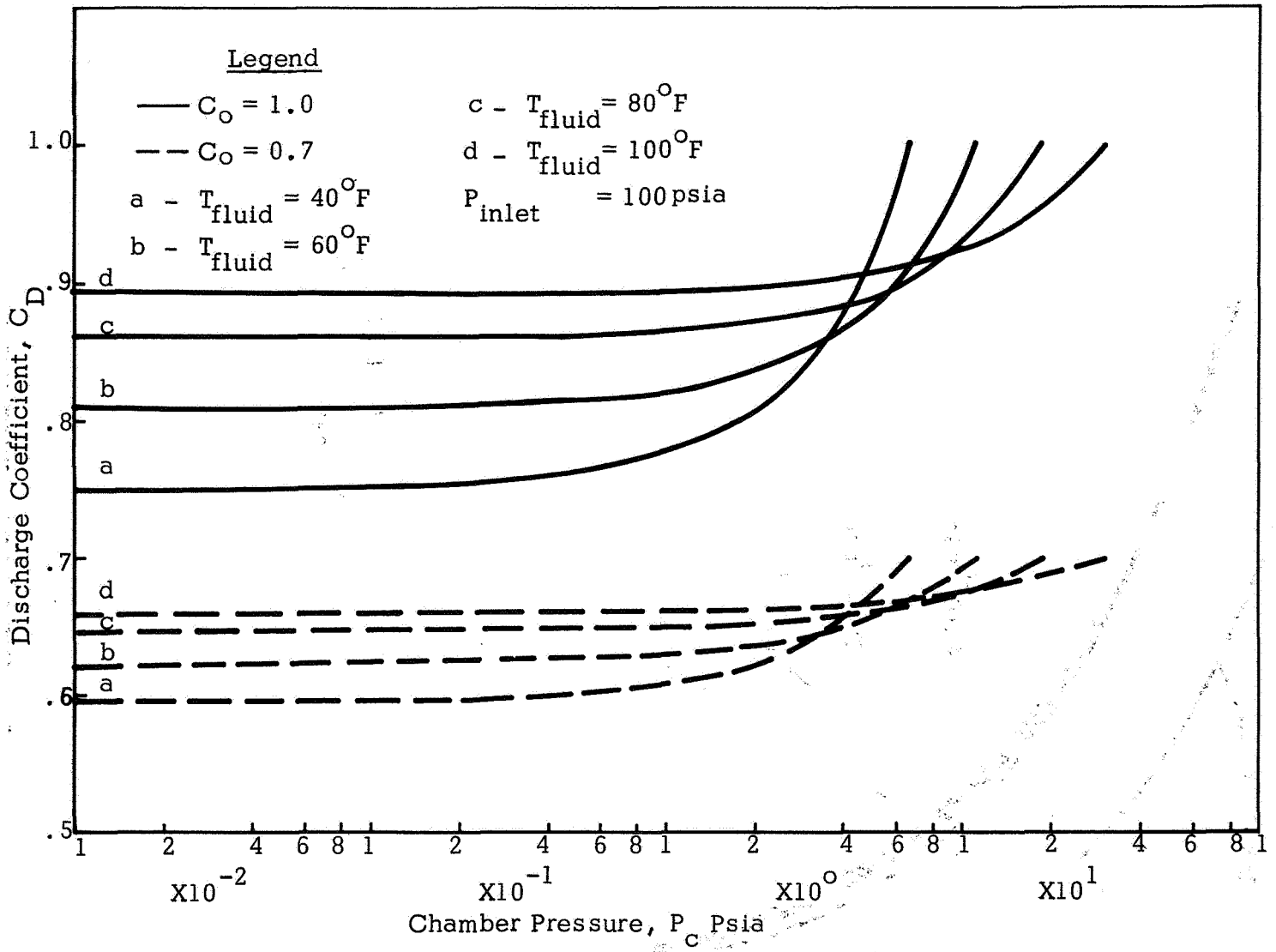

Figure 6. Theoretical Cavitating Discharge Coefficient Showing the Effects of the Orifice Discharge Coefficient, C_o.

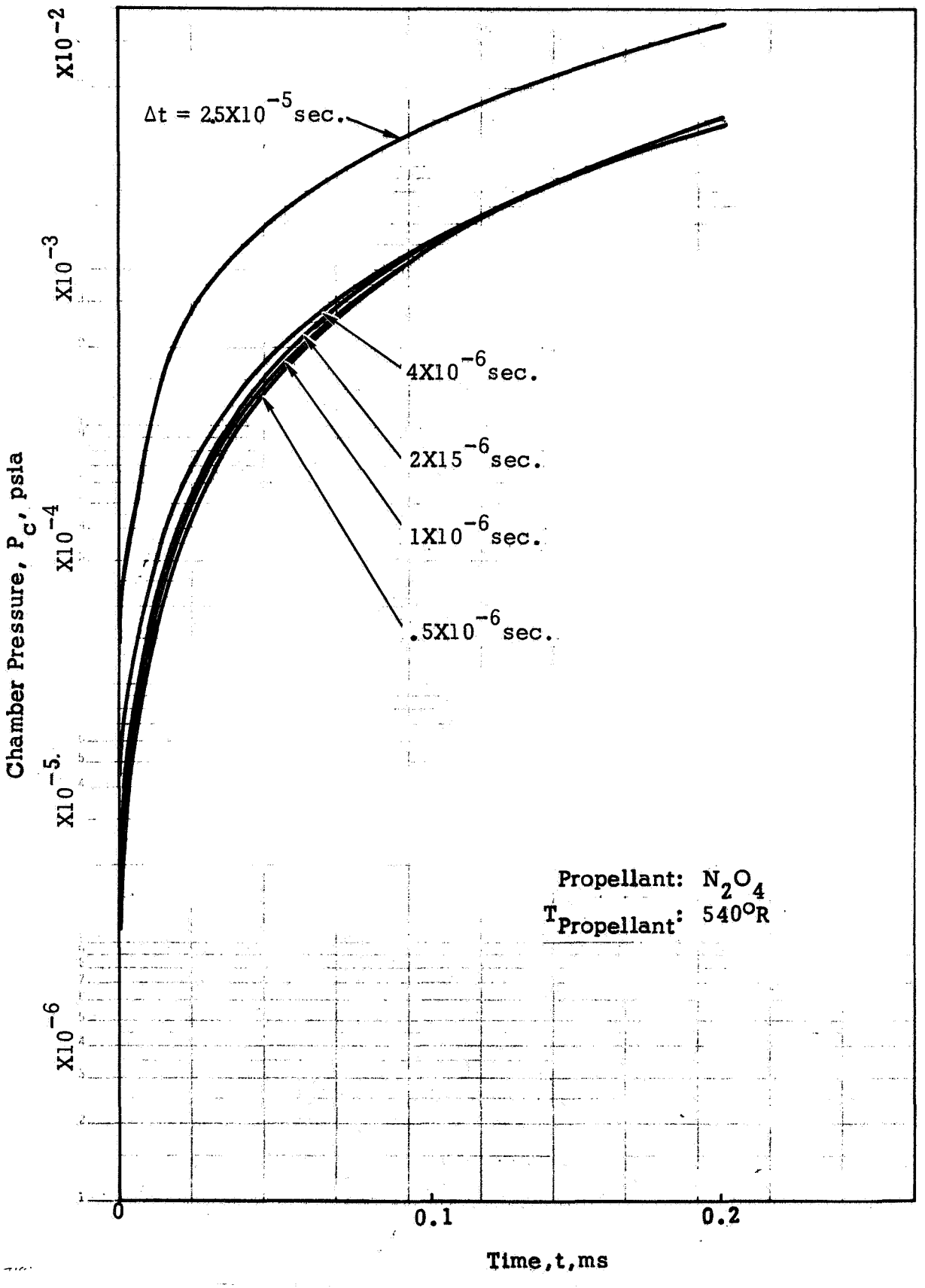

Figure 7. Effect of Integration Step on Chamber Pressurization

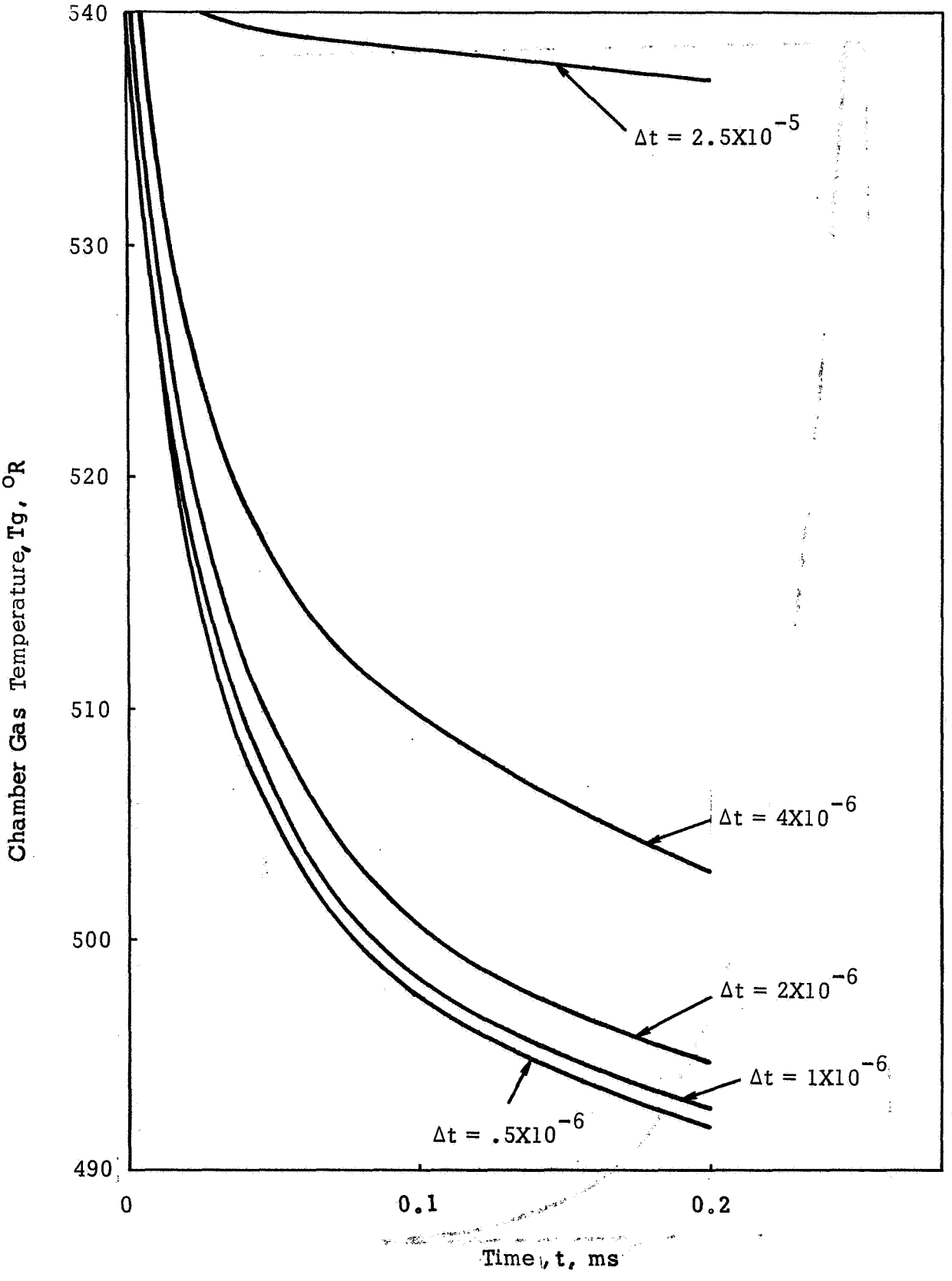

Figure 8. Effect of Integration Step on Chamber Gas Temperature

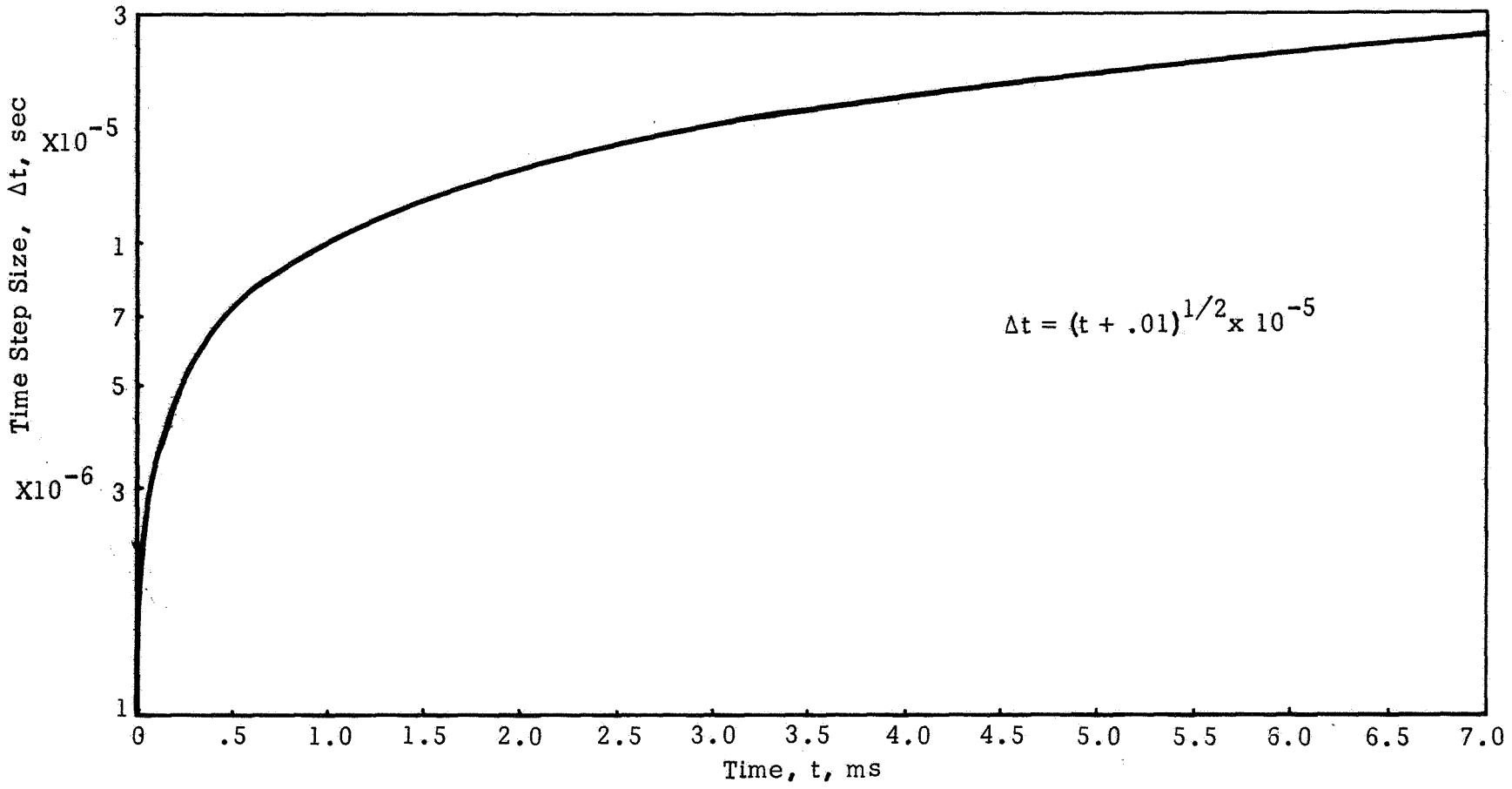

Figure 9. Variable Time Step Scheme Used in the N_2O_4 Space Start Program

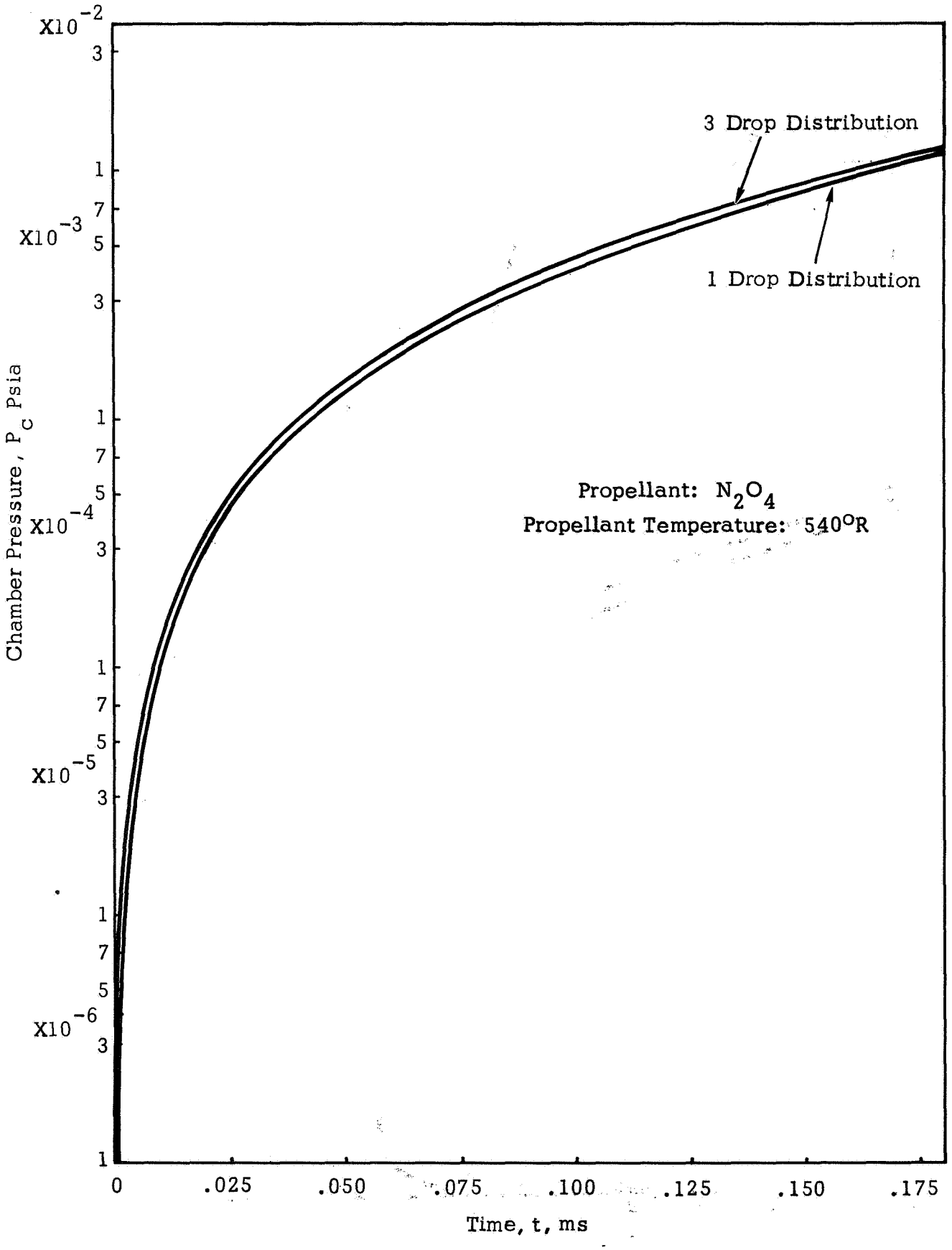

Figure 10. Effect of The Drop Size Distribution On The N_2O_4 Vaporization Model

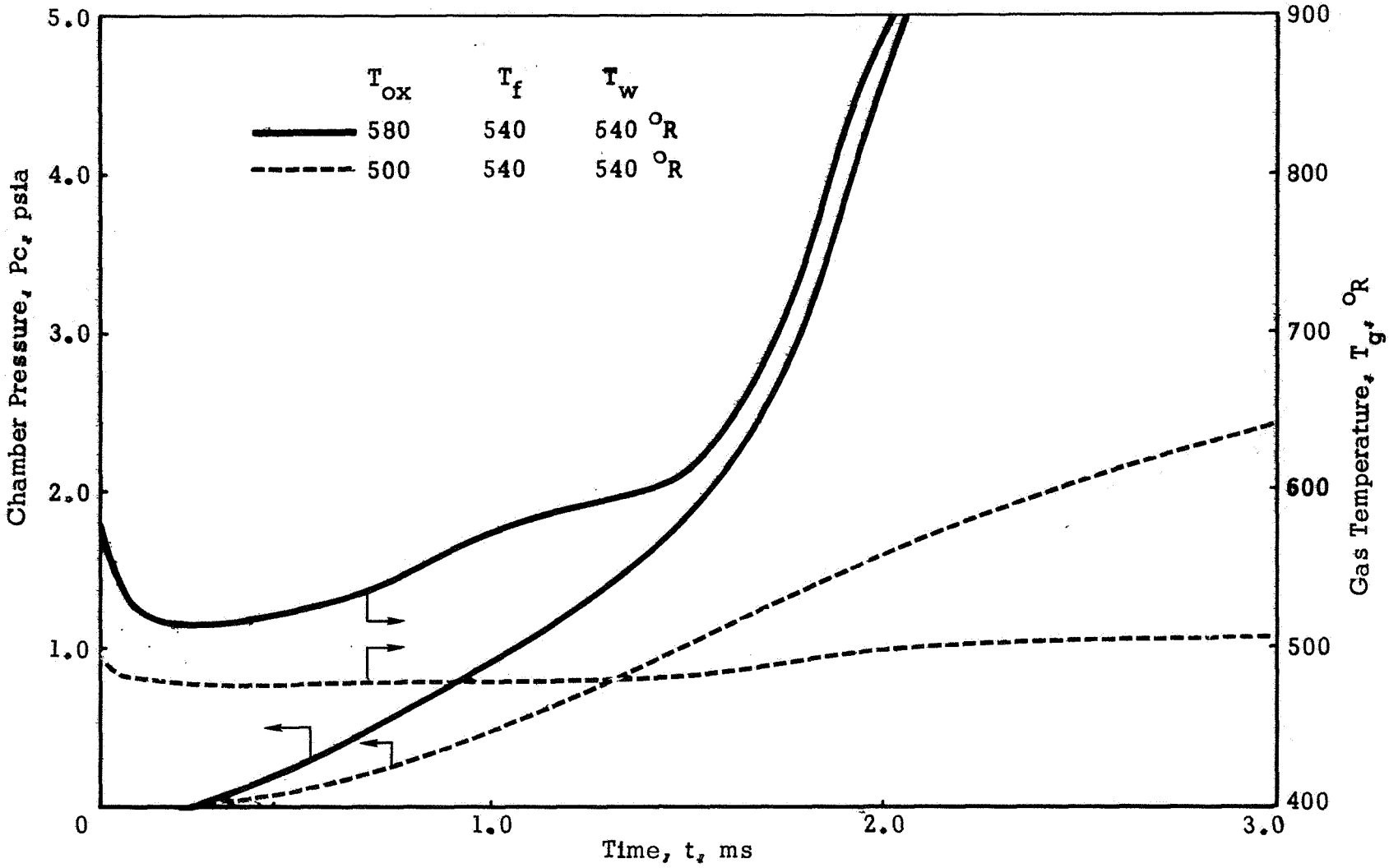

Figure 11. The Effect of Variable Oxidizer Temperature on Transient Chamber Pressure and Chamber Gas Temperature

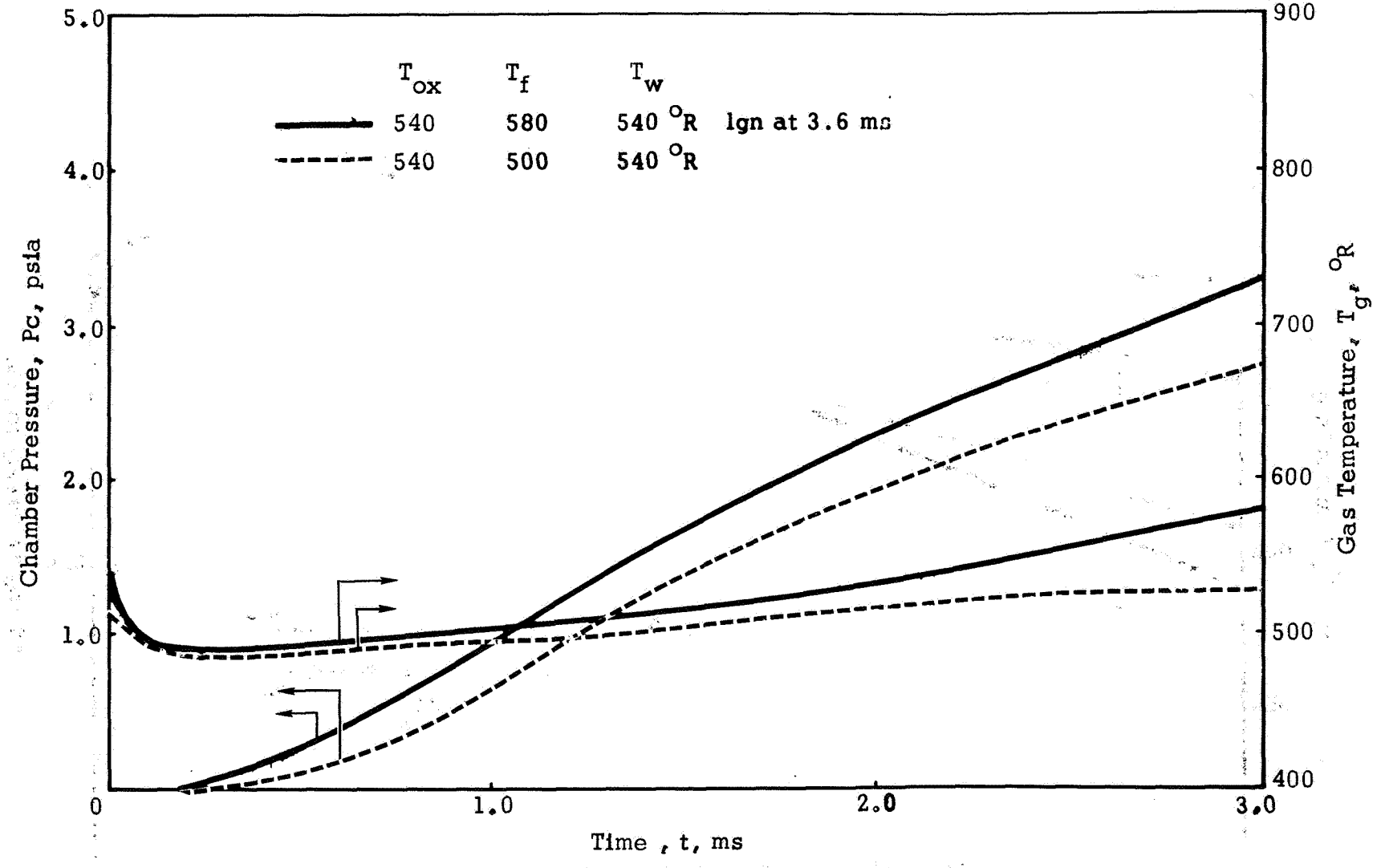

Figure 12.The Effect of Variable Fuel Temperature on Transient Chamber Pressure and Chamber Gas Temperature

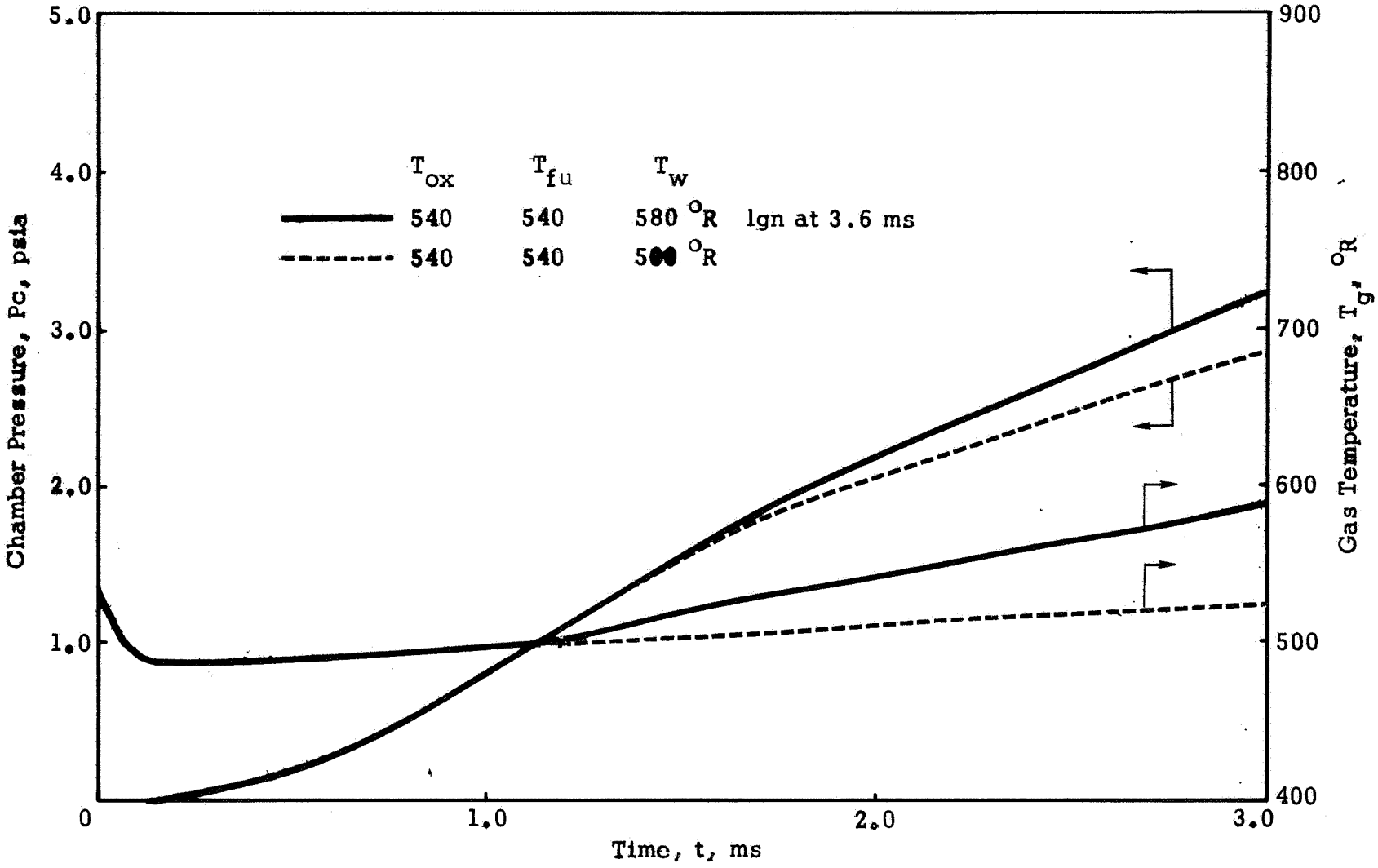

Figure 13. The Effect of Variable Wall Temperature on Transient Chamber Pressure and Chamber Gas Temperature

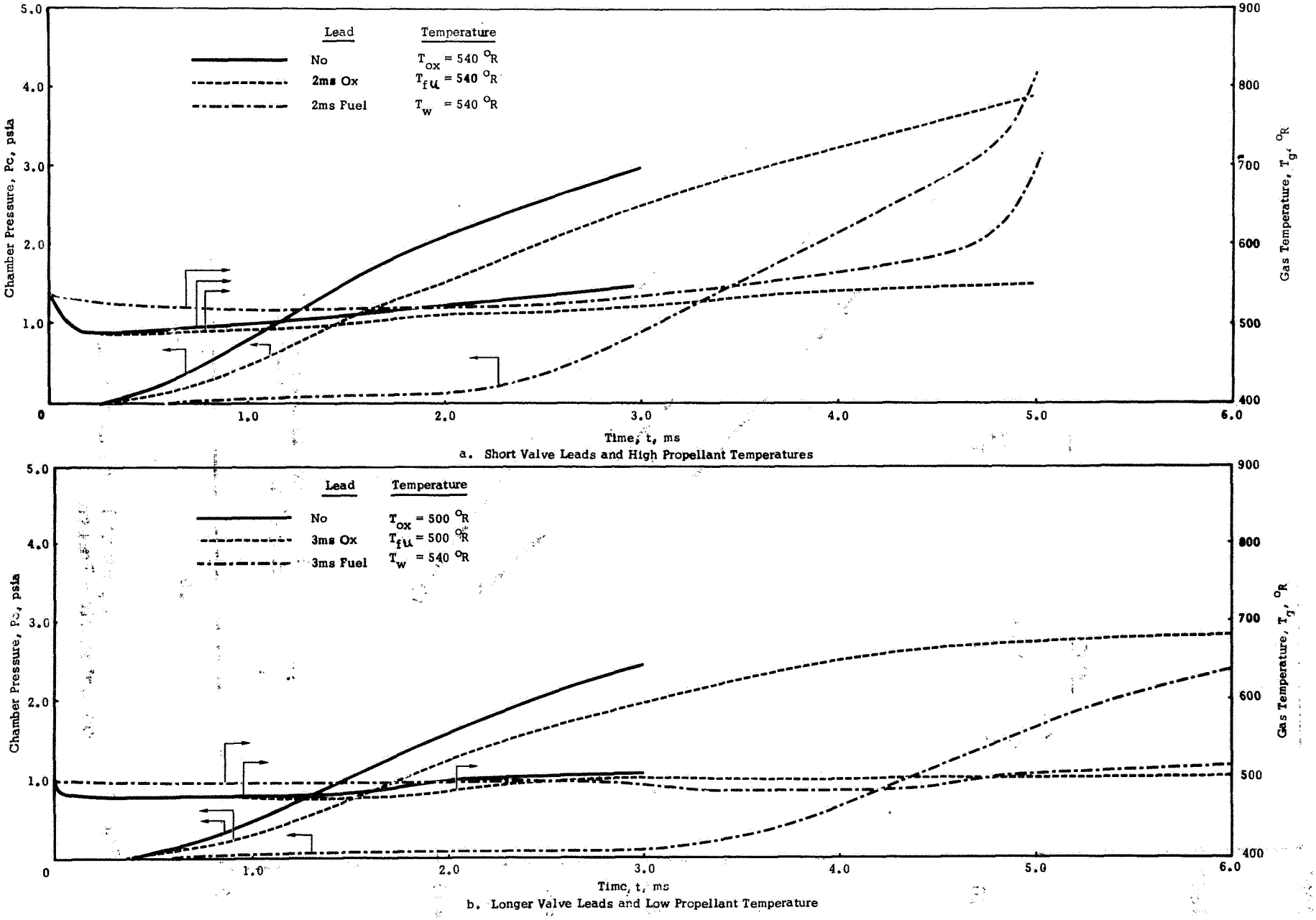

Figure 14. The Effect of Variable Valve Leads and Initial Temperature on Transient Chamber Pressure and Chamber Gas Temperature.

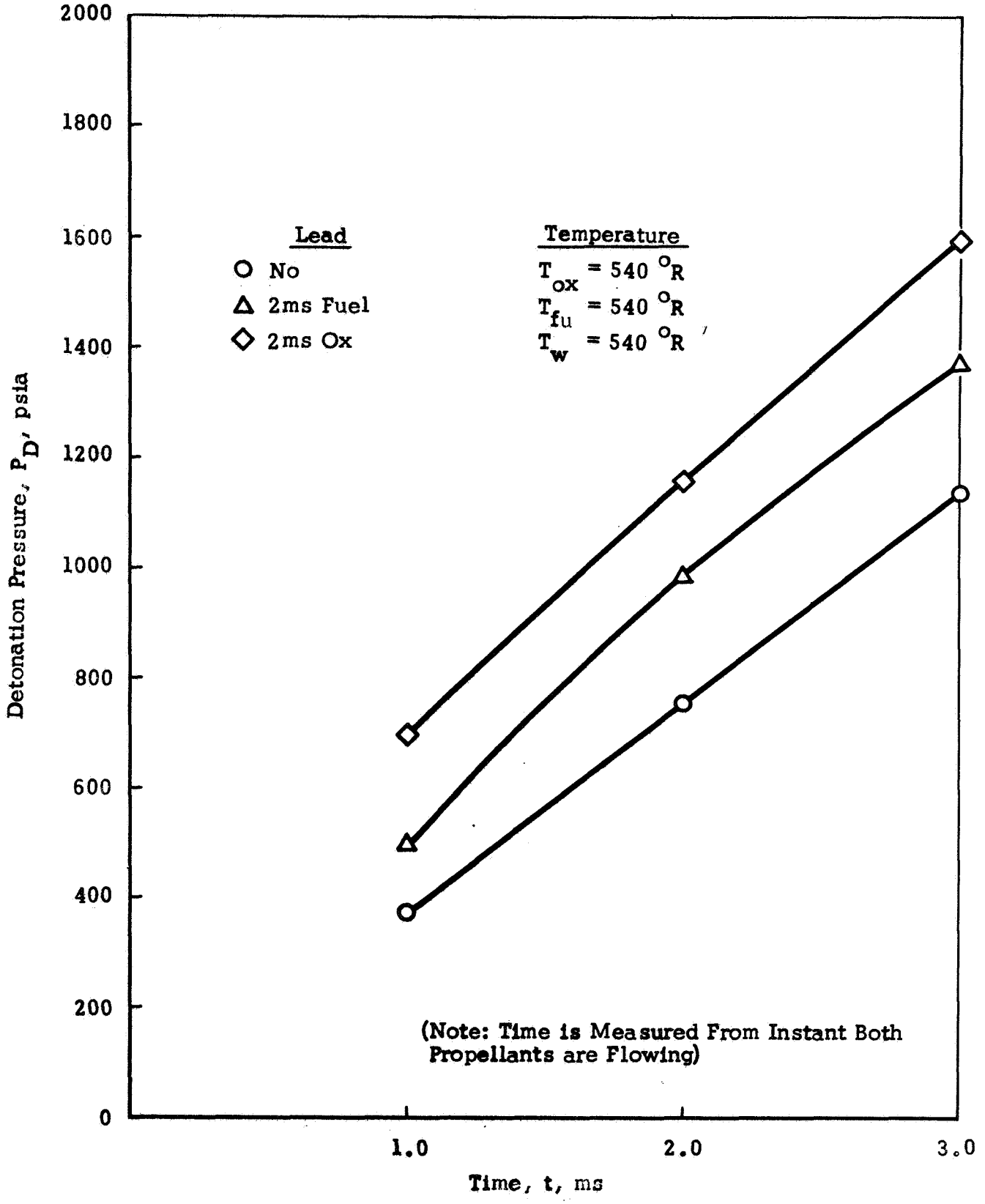

Figure 15. Effect of Propellant Leads and Initial Temperature on Detonation Pressure

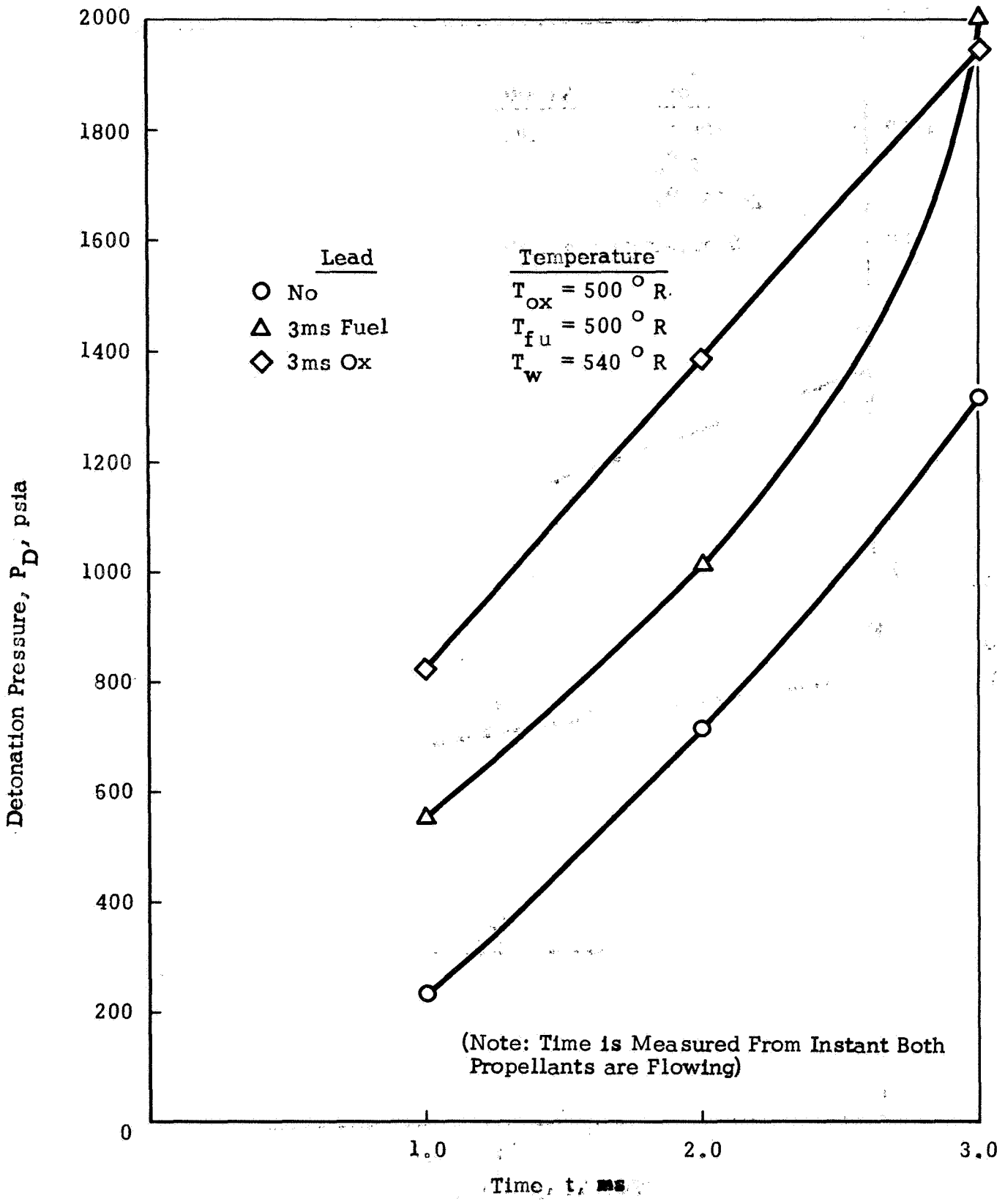

Figure 16. **Effect of Propellant Leads and Initial Temperature on Detonation Pressure**

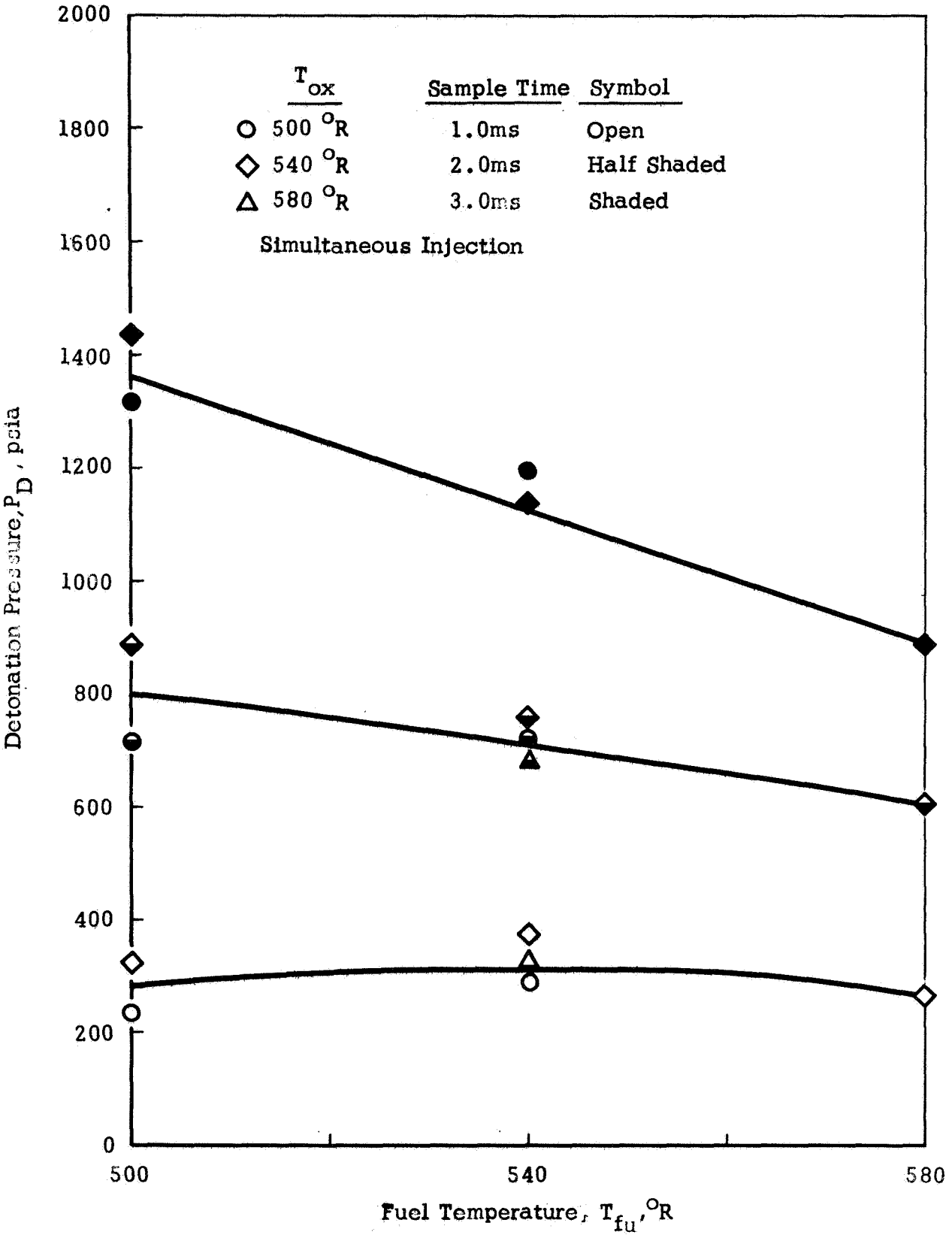

Figure 17. Effect of Fuel Temperature on Detonation Pressure

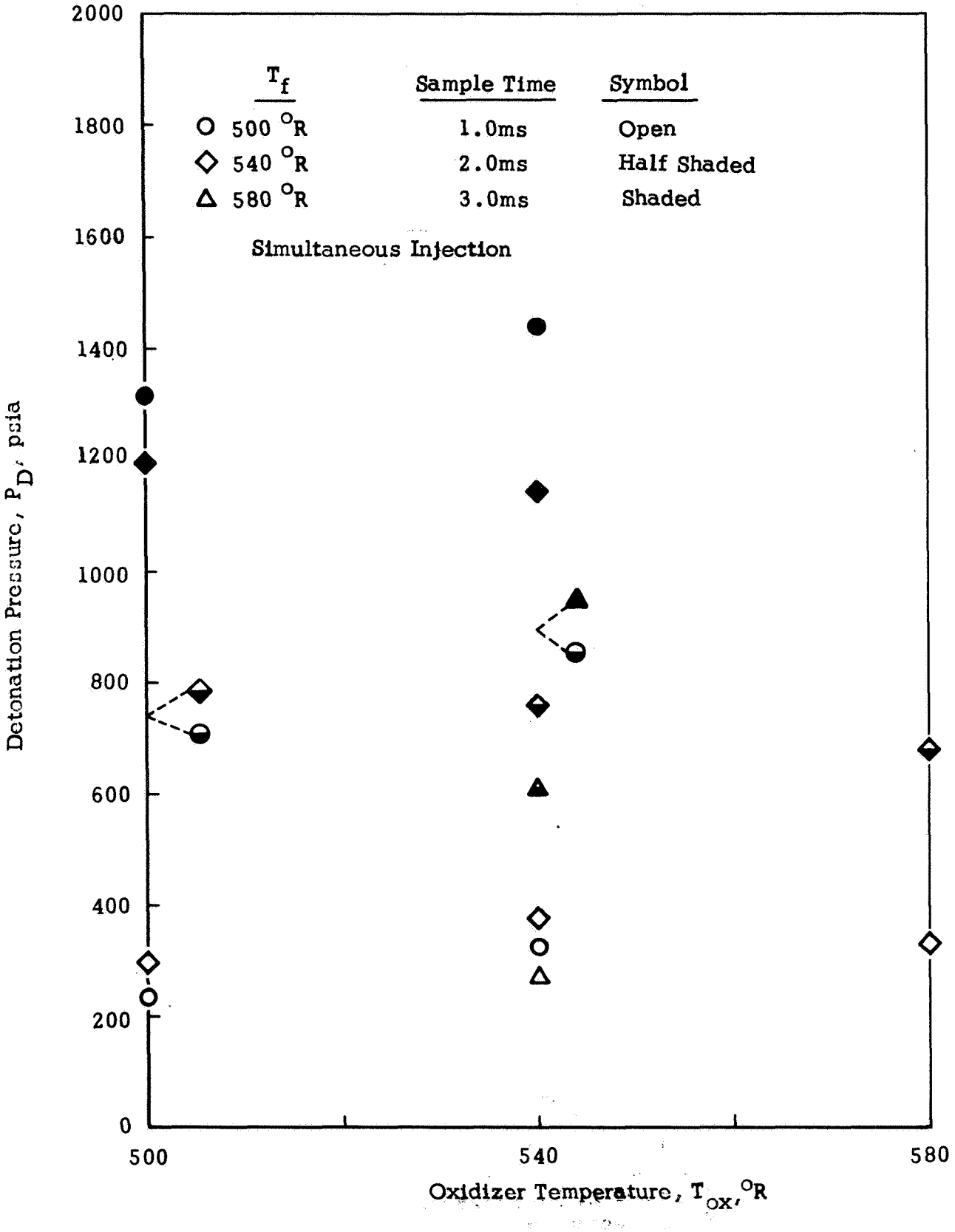

Figure 18. Effect of Oxidizer Temperature on Detonation Pressure

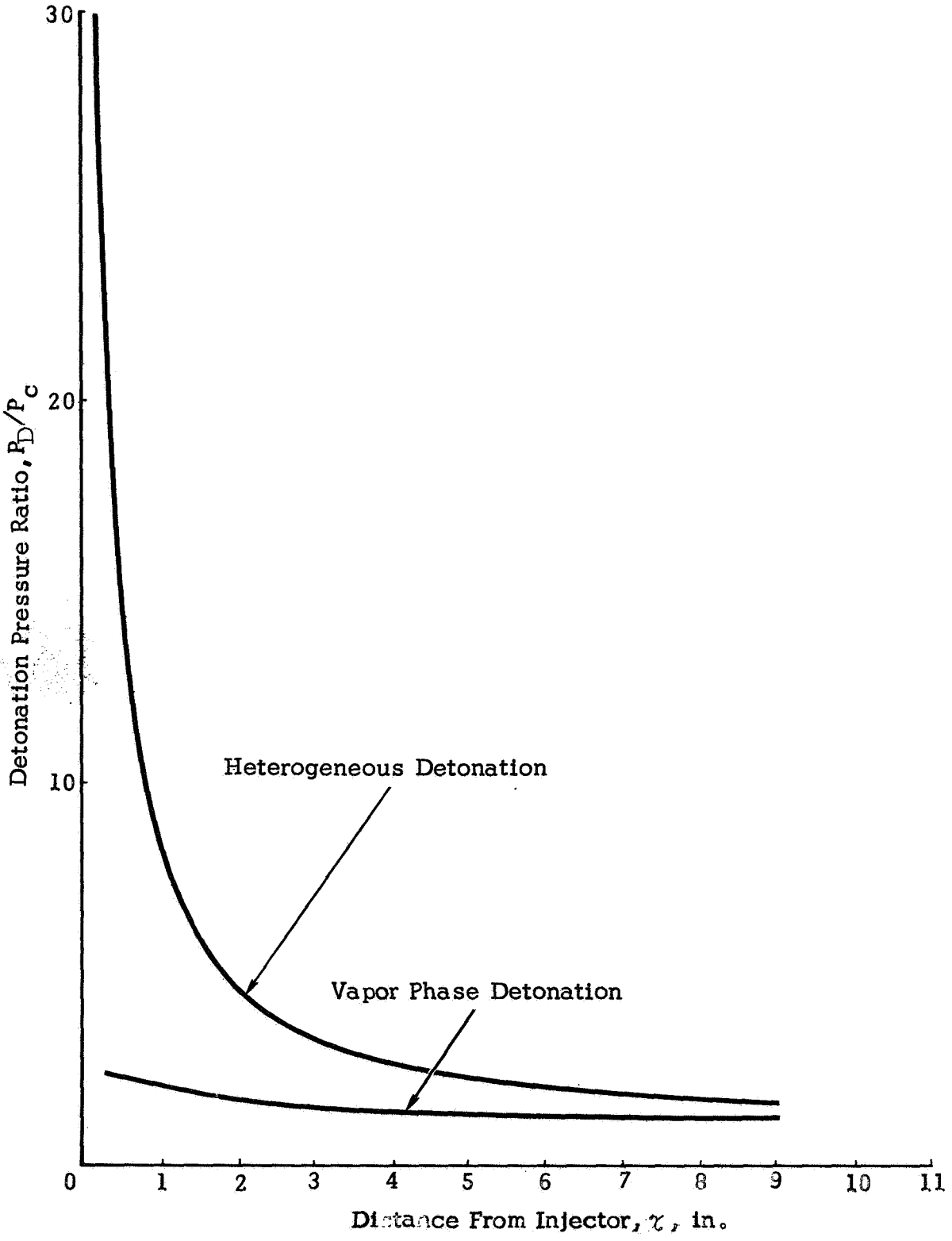

Figure 19. Detonation Pressure Ratio Versus Distance From Injector Face

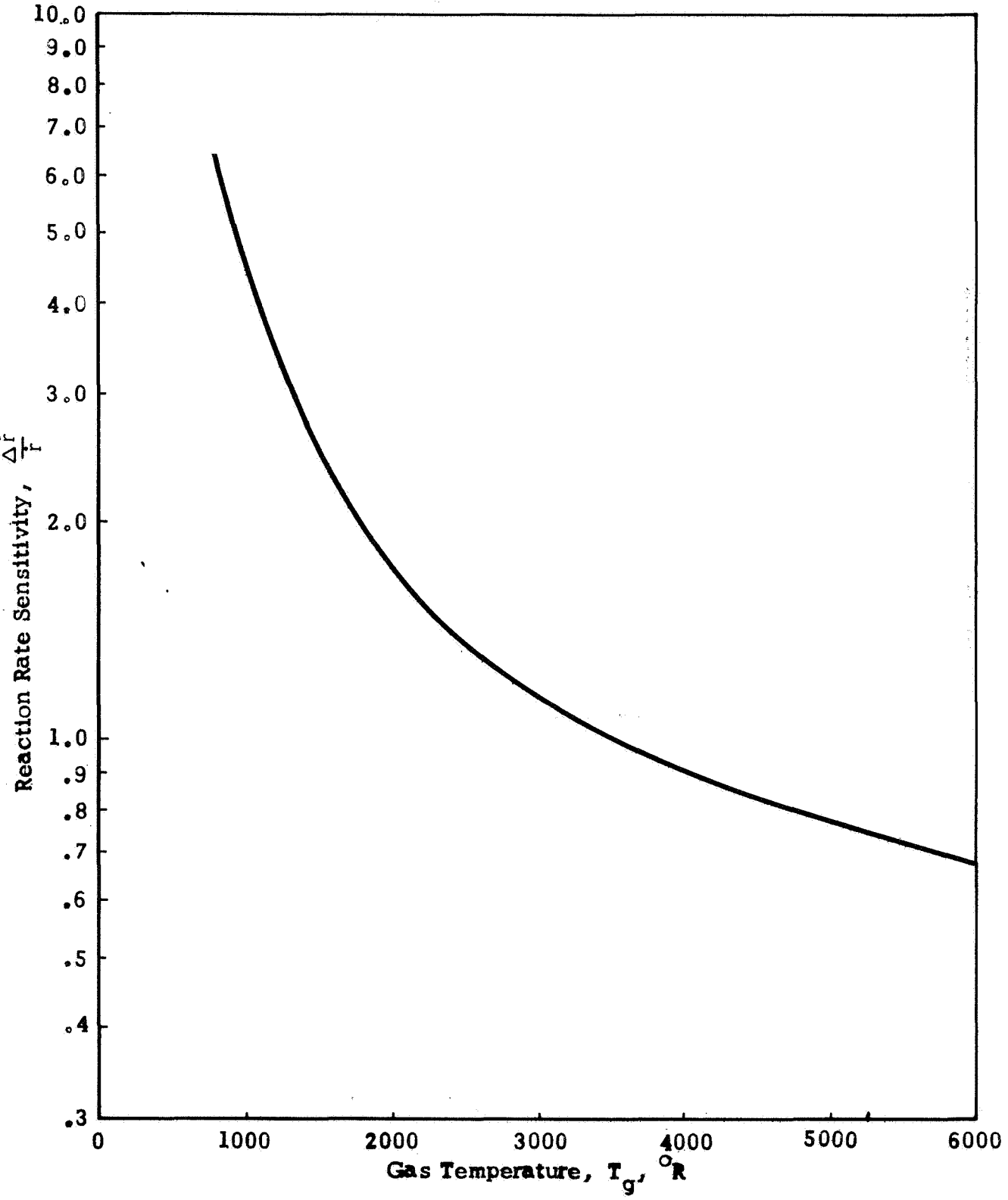

Figure 20. Reaction Rate Sensitivity Versus Gas Temperature

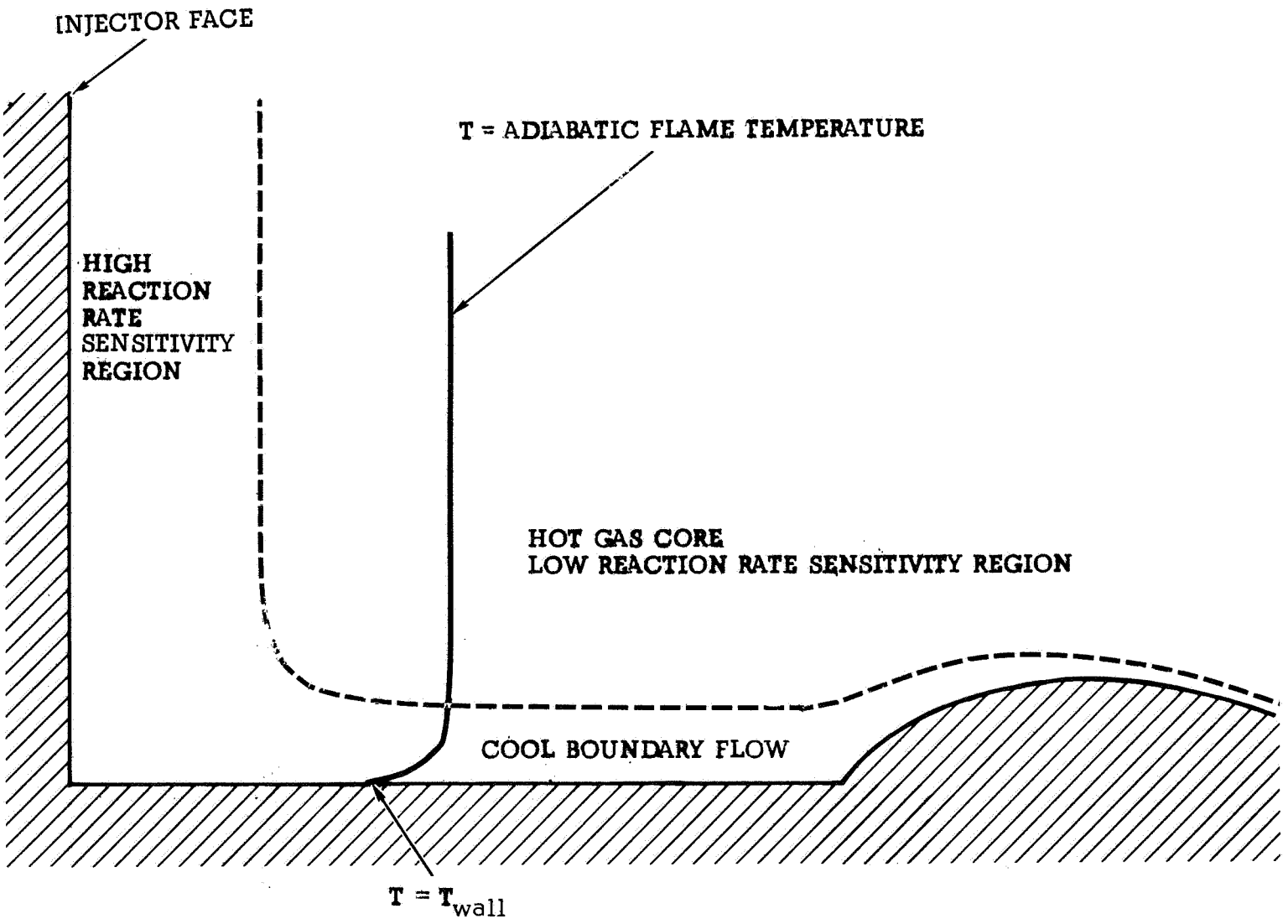

Figure 21. Rocket Engine Sensitivity Regions

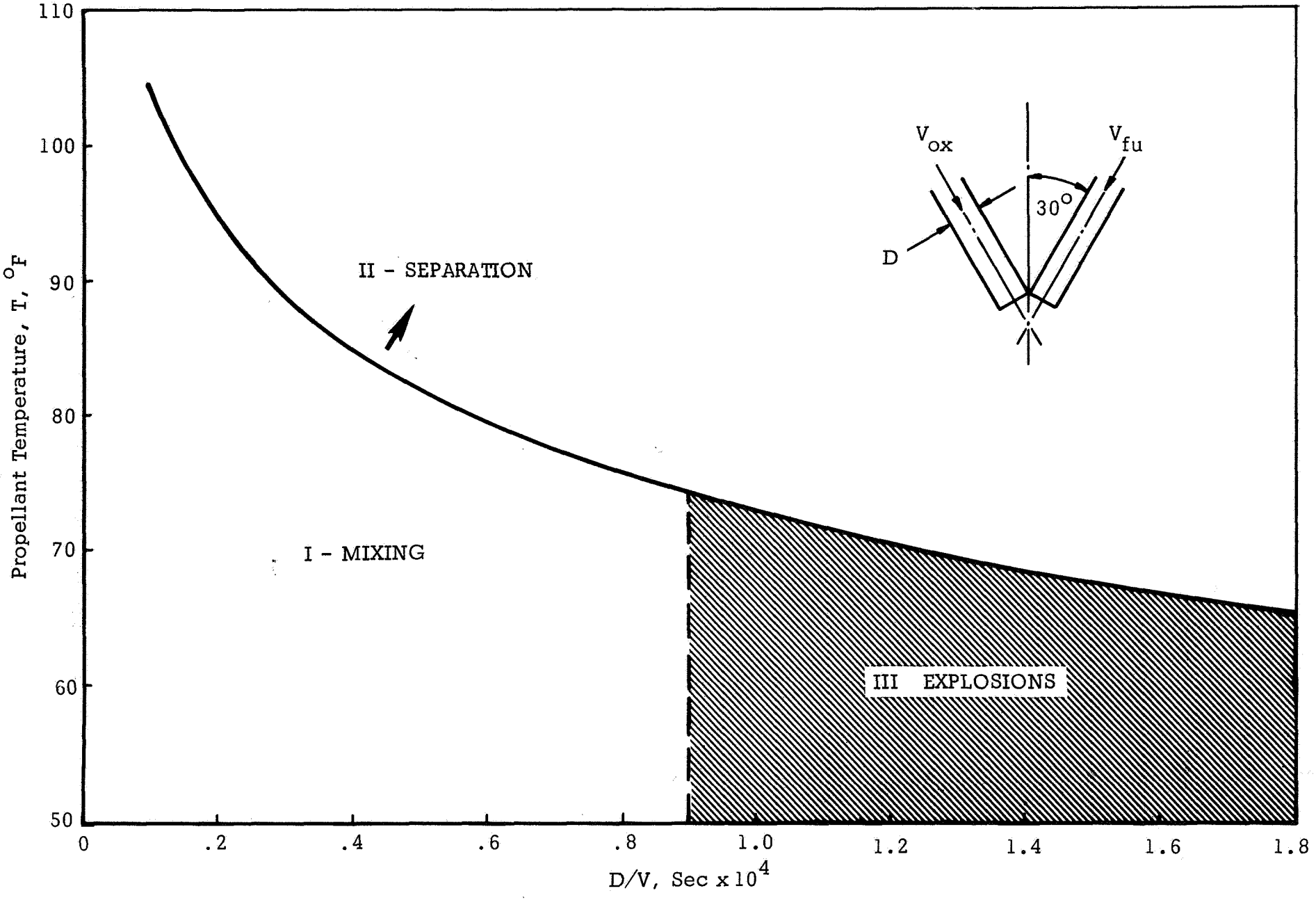

Figure 22. Jet Separation, Mixing, and Injector Mixing Explosions for Impinging N_2O_4/N_2H_4 /Streams.

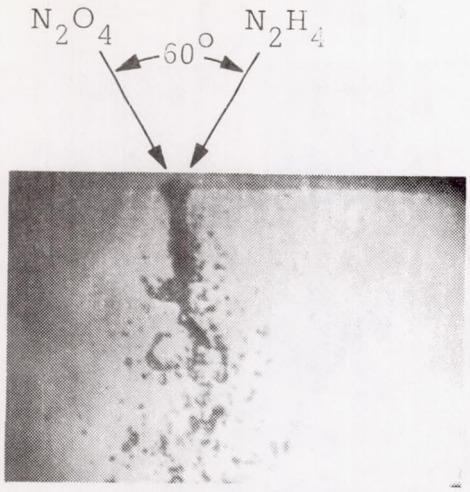

(1) TYPICAL SPRAY

(1) TYPICAL SPRAY

(2) INJECTION MIXING EXPLOSION

(2) INJECTION MIXING EXPLOSION

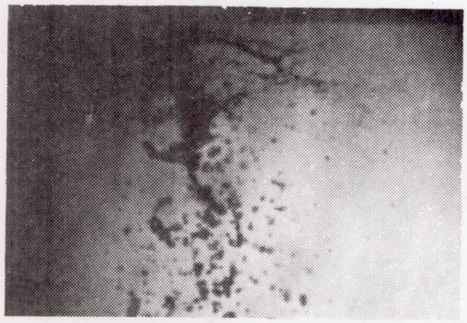

(3) LIGAMENT SHATTERING

INJECTION MIXING EXPLOSION
CAUSING LIGAMENT SHATTERING

(3) SPRAY DETONATION

INJECTION MIXING EXPLOSION
CAUSING SPRAY DETONATION

N_2H_4 VELOCITY = 25 ft/sec

N_2O_4 VELOCITY = 20 ft/sec

N_2H_4 ORIFICE DIA = .050"

N_2O_4 ORIFICE DIA = .050"

PROPELLANT TEMPERATURE 60°F

25 μsec EXPLOSURE AT 2000 pic/sec

Figure 23. Injection Mixing Explosions Leading to Either Ligament Shattering or Spray Detonation (Pop).

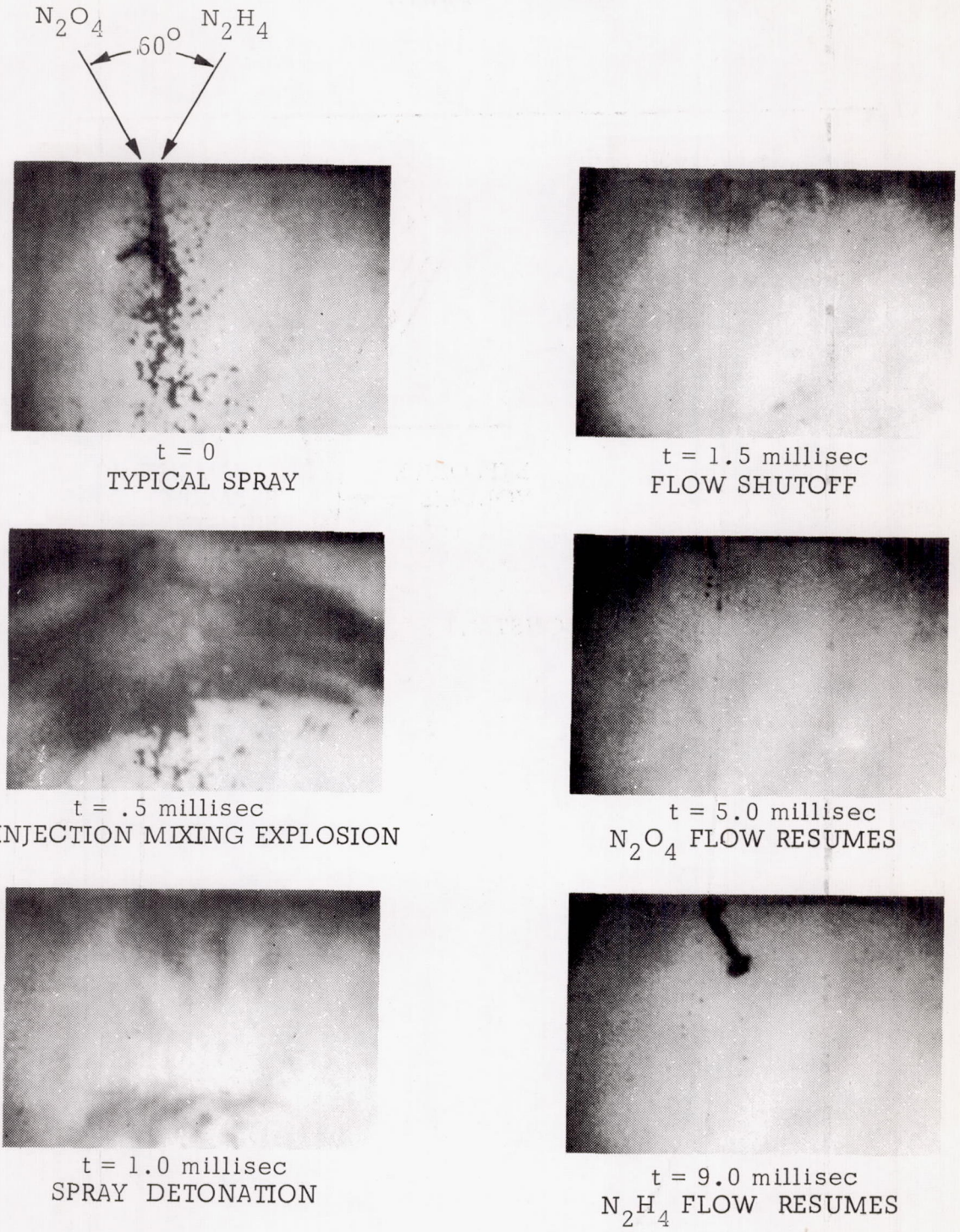

N_2H_4 VELOCITY = 25 ft/sec
N_2O_4 VELOCITY = 20 ft/sec

N_2H_4 ORIFICE DIA = .050"
N_2O_4 ORIFICE DIA = .050"

PROPELLANT EMPERATURE 60°F
25 μsec EXPOSURE at 2000 pic/sec

Figure 24. N_2O_4/N_2H_4 Injection Mixing Explosion Leading to Spray Detonation.

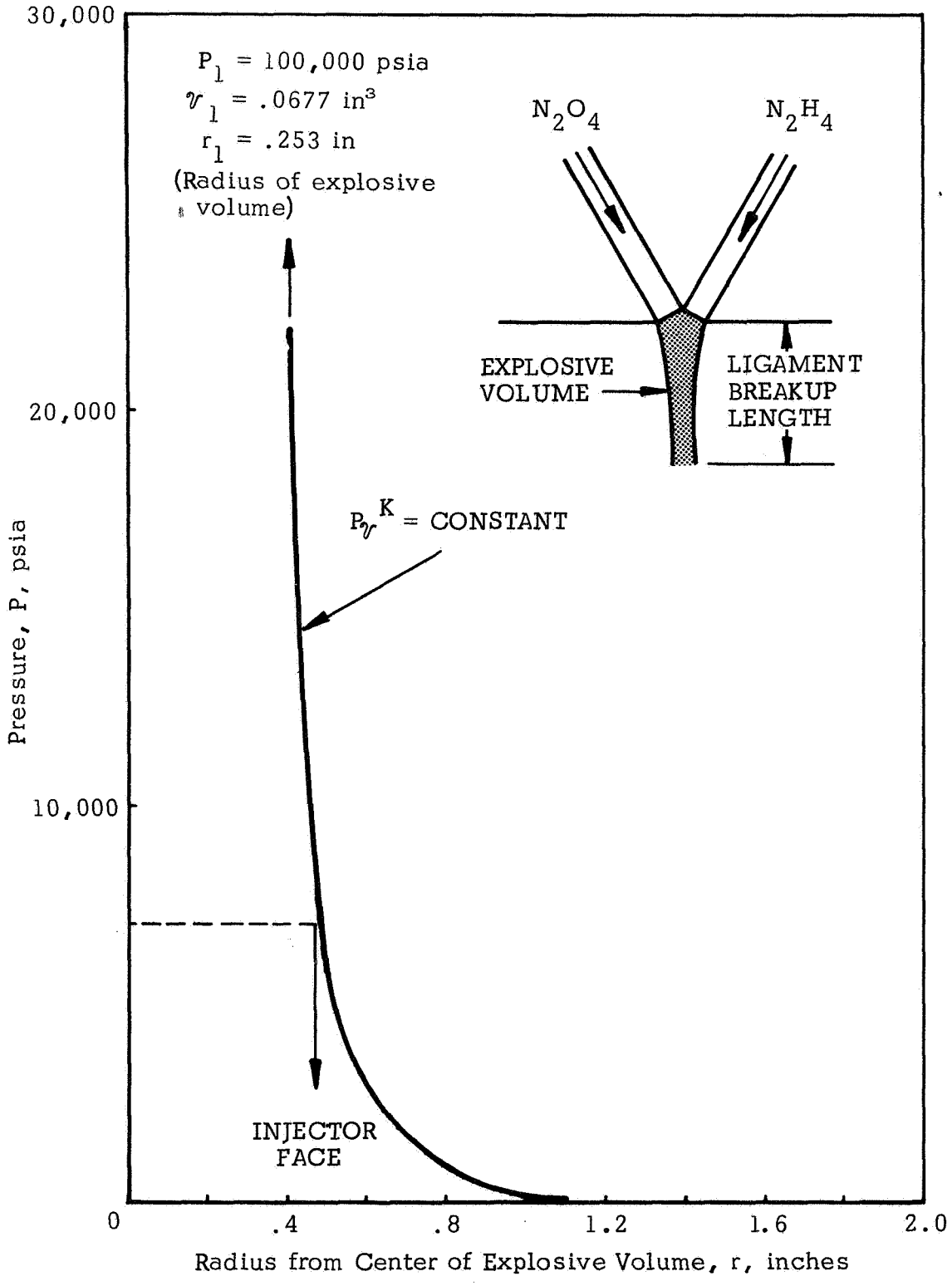

Figure 25. Pressure Decay of an Injector (POP).

Chief, Liquid Propulsion Technology (RPL) - NASA 4*
Washington, D.C. 20546

Director, Launch Vehicles and Propulsion, Services, NASA
Washington, D.C. 20546

Director, Advanced Manned Missions, Mt. NASA
Washington, D. C. 20546

Director, Mission Analysis Division
NASA-Ames Research Center
Moffett Field, Calif. 24035

Jet Propulsion Laboratory 5
4800 Oak Grove Drive
Pasadena, California 91103
Attn: R. M. Clayton

NASA Pasadena Office
4800 Oak Grove Drive
Pasadena, Calif. 91103
Attn: Contracting Officer
Attn: Office of Technical Information and Patent Matters

Scientific and Technical Information 25
Facility
Attn: NASA Representative, Code CRT
P.O.Box 33
College Park, Maryland 20740

Ames Research Center 2
Moffett Field, Calif.94035
Attn: Mr.Clarence A.Syvertson

Goddard Space Flight Center
Greenbelt, Maryland 20771
Attn: Merland L. Moseson, Code 620

Jet Propulsion Laboratory
4800 Oak Grove Drive
Pasadena, Calif. 91103
Attn: Henry Burlage, Jr.
Propulsion Division

Langley Research Center
Langley Station
Hampton, Virginia 23365
Attn: Dr. Floyd L. Tompson, Director

Lewis Research Center 2
21000 Brookpark Road
Cleveland, Ohio 44135
Attn: Dr. Abe Silverstein, Director

Lewis Research Center 2
21000 Brookpark Road
Cleveland, Ohio 44135
Attn: Dr. R. J. Priem

Marshall Space Flight Center 2
Huntsville, Alabama 35812
Attn: Hans G. Paul, Code R-P+VED
Werner Voss R-P and VE-PM

Manned Spacecraft Center 3
Houston, Texas 77058
Attn: J. G. Thibodaux, Jr., Code EP
Kieth Chandler, Librarian
H. Pohl, Code PSED Energy
Cecil Gibson

John F. Kennedy Space Center 2
NASA
Cocoa Beach, Florida 32931
Attn: Dr. Kurt H. Debus

NASA Test Facility
Propulsion Engineering Office
White Sands, N. M.
Attn: I.D. Smith, Staff Chemist

Government Installations

Aeronautical Systems Division
Air Force Systems Command
Wright-Patterson Air Force Base
Dayton, Ohio 45433
Attn: D. L. Schmidt, Code ASRCNC-2

Air Force Missile Development Center
Holloman Air Force Base
New Mexico 88330
Attn: Maj. R. E. Bracken, Code MDGRT

*One copy unless otherwise designated.
Copies sent direct to first section (NASA)
All others sent to librarian with copy of letter to addressee.

Air Force Missile Test Center
Patrick Air Force Base, Florida
Attn: L. J. Ullian

Air Force Systems Division
Air Force Unit Post Office
Los Angeles 45, Calif. 90045
Attn: Col. Clark, Tech.Data Center

AFFTC (FTBPP-2) 2
Edwards AFB, Calif. 93523
Attn: Myrtle C.Jones

Arnold Engineering Development Center
Arnold Air Force Station
Tullahoma, Tenn. 37388
Attn: Dr. H.K.Doetsch

Bureau of Naval Weapons
Department of the Navy
Washington, D.C. 20546
Attn: J. Kay, RTMS-41

Defense Documentation Center Headquarters
Cameron Station, Bldg. 5
5010 Duke Street
Alexandria, Va. 22314
Attn: TISIA

Headquarters, U.S.Air Force
Washington 25, D.C. 20546
Attn: Col. C.K.Stambaugh, AFRST

Picatinny Arsenal
Dover, N.J. 07801
Attn: I. Forsten, Chief Liq. Prop.Lab. SMUPA-DL

Air Force Rocket Propulsion Lab 2
Research and Technology Division
Air Force Systems Command
Edwards, Calif 93523
Attn: RPRPD/Mr.J.Lawrence

U.S.Atomic Energy Commission
Technicai Information Services
Box 62,
Oak Ridge, Tenn. 37830
Attn: A.P.Huber, Oak Ridge Gaseous Diffusion Plant (ORGDP)P.O.Box P

U.S.Army Missile Command
Redstone Arsenal
Alabama 35809
Attn: Dr. Walter Wharton

U.S.Naval Ordnance Test Station
China Lake, Calif. 93557
Attn: Code 4562, Chief, Missile Propulsion Division

Air Force Rocket Propulsion Lab
Research and Technology Division
Air Force Systems Command
Edwards, Calif. 93523
Attn: Capt. C.J.Abbe, RPRRC

U.S.Bureau of Mines
4800 Forbes Avenue
Pittsburgh, Penn. 15213
Attn: Mr. Henry Perlee

Chemical Propulsion Information Agency
Applied Physics Laboratory
8621 Georgia Avenue
Silver Spring, Maryland 20910
Attn: P. Martin

Industry Contractors

Aerojet-General Corporation
P.O.Box 296
Azusa, Calif. 91703

Aerojet-General Corporation
P.O.Box 1947
Technical Library, Bldg. 2015,Dept. 2410
Sacramento, Calif. 95809
Attn: R. Stiff
Dr. C. B. McGough

Aeronutronic Division
Philco Corporation
Ford Road
Newport Beach, Calif. 92663
Attn: Mr N. Stern

Aerospace Corporation
2400 East El Segundo Blvd.
P.O.Box 95085
Los Angeles, Calif. 90045
Attn: Mr. M.J.Russi
Dr. Leroy Schieler
Hideyo H. Takimoto

Airesearch Mfg. Co.
9851 Sepulveda Blvd.
Los Angeles, Calif. 90045
Attn: Mr. C. S. Coe

Arthur D. Little, Inc.
20 Acorn Park
Cambridge, Mass. 02140
Attn: Mr. E. K, Bastress

Astropower Laboratory
Douglas Aircraft Company
2121 Paularino
Newport Beach, Calif. 92663
Attn: Dr. George Moc
Director, Research

Astrosystems International, Inc.
1275 Bloomfield Avenue
Fairfield, New Jersey 07007
Attn: A. Mendenhall

Atlantic Research Corporation
Edsall Road and Shirley Highway
Alexandria, Virginia 22314
Attn: A. Scurlock
John Simmons

Beech Aircraft Corporation
Boulder Division
Box 631
Boulder, Colorada 80302
Attn: J. H. Rodgers

Bell Aerosystems Company
P. O. Box 1
Buffalo, New York 14240
Attn: Mr. N. Safeer
L. M. Wood

Bendix Systems Division
Bendix Corporation
3300 Plymouth Road
Ann Arbor, Michigan 48105
Attn: John M. Brueger

Boeing Company
P. O. Box 3707
Seattle, Washington 98124
Attn: J. D. Alexander

Missile Division
Chrysler Corporation
P. O. Box 2628
Detroit, Michigan 48231
Attn: Mr. John Gates

Wright Aeronautical Division
Curtiss-Wright Corporation
Wood-Ridge, New Jersey 07075
Attn: G. Kelley

Missile and Space Systems Division
Douglas Aircraft Company, Inc.
3000 Ocean Park Boulevard
Santa Monica, Calif. 90406
Attn: Mr. R. W. Hallet, Chief Engineer
Adv. Space Tech.
Mr. A. Pisciotta, Jr.

Aircraft Missiles Division
Fairchild Hiller Corporation
Hagerstown, Maryland 21740
Attn: J. S. Kerr

General Dynamics
Convair Division
5001 Kearny Villa Road
P. O. Box 1628
San Diego, Calif. 92112
Attn: E. R. Peterson
V. P., Research and Eng.

Missile and Space Systems Center 2
General Electric Company
Valley Forge Space Technology Center
P. O. Box 8555
Philadelphia, Pa.
Attn: F. Mezger
Reentry Systems Dept.

Advanced Engine & Technology Dept.
General Electric Company
Cincinnati, Ohio 45215
Attn: D. Suichu

Grumman Aircraft Engineering Corp.
Bethpage, Long Island
New York 11714
Attn: Joseph Gavin

Honeywell, Inc.
Aerospace Div.
2600 Ridgway Rd.
Minneapolis, Minn.
Attn: Mr. Gordon Harms

Hughes Aircraft Co.
Aerospace Group
Centinela and Teale Streets
Culver City, Calif.
Attn: E. H. Meier
V. P., and Div. Mgr.,
Research and Dev. Div.

Walter Kidde and Company, Inc.
Aerospace Operations
567 Main Street
Belleville, New Jersey
Attn: Mr. R. J. Hanville
Dir. of Research Engr.
Mr. K. A. Traynellis

Ling-Temco-Vought Corporation
Astronautics
P. O. Box 5907
Dallas, Texas 75222
Attn: Garland Whisenhunt

Lockheed Missiles and Space Co.
Attn: Technical Information Center
P. O. Box 504
Sunnyvale, California 94088
Attn: Y. C. Lee

Lockheed Propulsion Company
P. O. Box 111
Redlands, California 92374
Attn: H. L. Thackwell

The Marquardt Corporation
16555 Saticoy Street
Van Nuys, Calif. 91409
Attn: Warren P. Boardman, Jr.
Warren Juran

Baltimore Division
Martin Marietta Corporation
Baltimore, Maryland 21203
Attn: Mr. John Calathes (3214)

Denver Division
Martin Marietta Corporation
P. O. Box 179
Denver, Colorado 80201
Attn: J. D. Goodlette (A-241)
A. J. Kullas

Orlando Division
Martin Marietta Corporation
Box 5837
Orlando, Florida
Attn: Mr. J. Ferm

McDonnell-Douglas Aircraft Corp.
P. O. Box 516
Municipal Airport
St. Louis, Missouri 63166
Attn: R. A. Herzmark
Mr. R. E. Martins

Space & Information Systems Division
North American Aviation, Inc.
12214 Lakewood Blvd.
Downey, California 90241
Attn: H. Storms

Rocketdyne (Library 586-306)
North American Aviation, Inc.
6633 Canoga Avenue
Canoga Park, Calif. 91304
Attn: E. B. Monteath
S. D. Clapp

Northrop Space Laboratories
3401 West Broadway
Hawthorne, California 90250
Attn: Dr. William Howard

Reaction Motors Division
Thiokol Chemical Corporation
Denville, New Jersey 07832
Attn: Mr. Robert Parker
Mr. Robert Gere
Mr. Tom Seamans

Republic Aviation Corporation
Farmingdale, Long Island, New York
Attn: Dr. William O'Donnell

Space General Corporation
9200 East Flair Avenue
El Monte, California 91734
Attn: C. E. Roth

Stanford Research Institute
333 Ravenswood Avenue
Menlo Park, California 94025
Attn: Lionel Dickinson

TRW, Inc. 2
TRW Systems Group
One Space Park
Redondo Beach, Calif. 90278
Attn: Mr. D. Lee
Mr. V. Moseley

Tapco Division
TRW, Incorporated
23555 Euclid Avenue
Cleveland, Ohio 44117
Attn: P. T. Angell

Thiokol Chemical Corporation
Huntsville Division
Huntsville, Alabama 35807
Attn: John Goodloe

Research Laboratories
United Aircraft Corp.
400 Main Street
East Hartford, Conn. 06108

United Technology Center
587 Methilda Avenue
P. O. Box 358
Sunnyvale, California 94088
Attn: B. Adelman

Florida Research and Development
Pratt and Whitney Aircraft
United Aircraft Corporation
P. O. Box 2691
West Palm Beach, Florida 33402
Attn: R. J. Coar

Vickers, Inc.
Box 302
Troy, Michigan

Sunstrand Aviation
2421 11th Street
Rockford, Illinois 61101
Attn: Mr. R. W. Reynolds

Hamilton Standard Division
United Aircraft Corp.
Windsor Locks, Conn. 06096
Attn: Mr. R. Hatch

Rocket Research Corporation
520 South Portland Street
Seattle, Washington 98108
Attn: Foy McCullough, Jr.

Multi-Tech, Inc.
601 Glenoaks Blvd.
San Fernando, Calif. 91340
Attn: Mr. F. B. Cramer

Mathematical Applications Group, Inc.
180 So. Broadway
White Plains, New York 10605
Attn: Dr. S. Z. Burnstein

Universities

Ohio State University
Dept. of Aeronautical Eng.
Columbus, Ohio 43210
Attn: R. Edse

Pennsylvania State Univ.
Mech. Engineering Dept.
207 Mechanical Engineering Blvd.
University Park, Pa. 16802
Attn: G. M. Faeth

University of Southern Calif.
Dept. of Mech. Eng.
University Park
Los Angeles, Calif. 90007
Attn: M. Gerstein

Princeton University
Forrestal Campus
Guggenheim Laboratories
Princeton, New Jersey 08540
Attn: D. Harrje

University of Wisconsin
Mechanical Eng. Dept.
1513 University Avenue
Madison, Wisconsin 53705
Attn: P. S. Myers

University of Michigan
Aerospace Engineering
Ann Arbor, Michigan 48104
Attn: J. A. Nicholls

University of California
Dept. of Chemical Eng.
6161 Etcheverry Hall
Berkeley, Calif. 94720
Attn: A. K. Oppenhiem
R. Sawyer

Purdue University
School of Mech. Eng.
Lafayette, Indiana 47907
Attn: J. R. Osborn

Sacramento State College
Engineering Division
60000 J. Street
Sacramento, California 95819
Attn: E. H. Reardon

Massachusetts Institute of Tech.
Dept. of Mech. Eng.
Cambridge, Mass. 02139
Attn: T. Y. Toong

Illinois Institute of Technology
Rm. 200 M. H.
3300 S. Federal Street
Chicago, Illinois 60616
Attn: T. P. Torda

Polytechnic Institute of Brooklyn
Graduate Center
Route 110
Farmingdale, New York
Attn: V. D. Agosta

Georgia Institute of Technology
Atlanta, Georgia 30332
Attn: B. T. Zinn

University of Denver
Research Institute
Denver, Colorado
Attn: W. H. McClain

New York University
Dept. of Chem. Eng.
University Heights
New York, 53, New York
Attn: Leonard Dauerman